Uranium and molybdenum isotope evidence for an episode of widespread ocean oxygenation during the late Ediacaran Period

Brian Kendall[a,b,*], Tsuyoshi Komiya[b,c,d], Timothy W. Lyons[e], Steve M. Bates[e], Gwyneth W. Gordon[b], Stephen J. Romaniello[b], Ganqing Jiang[f], Robert A. Creaser[g], Shuhai Xiao[h], Kathleen McFadden[i], Yusuke Sawaki[j], Miyuki Tahata[k], Degan Shu[l], Jian Han[l], Yong Li[m], Xuelei Chu[n], Ariel D. Anbar[b,o]

[a] Department of Earth and Environmental Sciences, University of Waterloo, 200 University Avenue West, Waterloo, Ontario, Canada N2L 3G1

[b] School of Earth and Space Exploration, Arizona State University, Tempe, AZ 85287, USA

[c] Department of Earth Science and Astronomy, The University of Tokyo, 3-8-1 Komaba, Meguro-ku, Tokyo, 153-8902, Japan

[d] Research Center for the Evolving Earth and Planets, Tokyo Institute of Technology, 2-12-1 Ookayama, Meguro-ku, Tokyo 152-8551, Japan

[e] Department of Earth Sciences, University of California, Riverside, CA 92521, USA

[f] Department of Geoscience, University of Nevada, Las Vegas, NV 89154, USA

[g] Department of Earth and Atmospheric Sciences, University of Alberta, Edmonton, Alberta T6G 2E3, Canada

[h] Department of Geosciences, Virginia Polytechnic Institute and State University, Blacksburg, VA 24061, USA

[i] ConocoPhillips, Houston, TX 77079, USA

[j] Institute for Research on Earth Evolution, Japan Agency for Marine-Earth Science and Technology, 2-15 Natsushima-Cho, Yokosuka-city, Kanagawa 237-0061, Japan

[k] Department of Earth and Planetary Sciences, Tokyo Institute of Technology, 2-12-1 Ookayama, Meguro-ku, Tokyo, 152-8551, Japan

[l] Department of Geology and Key Laboratory for Continental Dynamics, Northwest University, Xi'an, 710069, China

[m] School of Earth Sciences and Resources Management, Chang'an University, Xi'an 710054, China

[n] Institute of Geology and Geophysics, Chinese Academy of Sciences, Beijing 100029, China

[o] Department of Chemistry and Biochemistry, Arizona State University, Tempe, AZ 85287, USA

Manuscript accepted for *Geochimica et Cosmochimica Acta*

2015

https://doi.org/10.1016/j.gca.2015.02.025

*Corresponding author at: Department of Earth and Environmental Sciences, University of Waterloo, 200 University Avenue West, Waterloo, Ontario, Canada N2L 3G1.

Email: bkendall@uwaterloo.ca

Abstract

To improve estimates of the extent of ocean oxygenation during the late Ediacaran Period, we measured the U and Mo isotope compositions of euxinic (anoxic and sulfidic) organic-rich mudrocks (ORM) of Member IV, upper Doushantuo Formation, South China. The average $\delta^{238}U$ of most samples is 0.24 ± 0.16 ‰ (2SD; relative to standard CRM145), which is slightly higher than the average $\delta^{238}U$ of 0.02 ± 0.12 ‰ for restricted Black Sea (deep-water Unit I) euxinic sediments and is similar to a modeled $\delta^{238}U$ value of 0.2 ‰ for open ocean euxinic sediments in the modern well-oxygenated oceans. Because ^{238}U is preferentially removed to euxinic sediments compared to ^{235}U, expanded ocean anoxia will deplete seawater of ^{238}U relative to ^{235}U, ultimately leading to deposition of ORM with low $\delta^{238}U$. Hence, the high $\delta^{238}U$ of Member IV ORM points to a common occurrence of extensive ocean oxygenation ca. 560 to 551 Myr ago.

The Mo isotope composition of sediments deposited from strongly euxinic bottom waters ($[H_2S]_{aq}$ > 11 μM) either directly records the global seawater Mo isotope composition (if Mo removal from deep waters is quantitative) or represents a minimum value for seawater (if Mo removal is not quantitative). Near the top of Member IV, $\delta^{98}Mo$ approaches the modern seawater value of 2.34 ± 0.10‰. High $\delta^{98}Mo$ points to widespread ocean oxygenation because the preferential removal of isotopically light Mo to sediments occurs to a greater extent in O_2-rich compared to O_2-deficient marine environments. However, the $\delta^{98}Mo$ value for most Member IV ORM is near 0‰ (relative to standard NIST SRM 3134 = 0.25‰), suggesting extensive anoxia. The low $\delta^{98}Mo$ is at odds with the high Mo concentrations of Member IV ORM, which suggest a large seawater Mo inventory in well-oxygenated oceans, and the high $\delta^{238}U$. Hence, we propose that the low $\delta^{98}Mo$ of most Member IV ORM was fractionated from contemporaneous seawater.

Possible mechanisms driving this isotope fractionation include: (1) inadequate dissolved sulfide for quantitative thiomolybdate formation and capture of a seawater-like δ^{98}Mo signature in sediments or (2) delivery of isotopically light Mo to sediments via a particulate Fe-Mn oxyhydroxide shuttle.

A compilation of Mo isotope data from euxinic ORM suggests that there were transient episodes of extensive ocean oxygenation that break up intervals of less oxygenated oceans during late Neoproterozoic and early Paleozoic time. Hence, Member IV does not capture irreversible deep ocean oxygenation. Instead, complex ocean redox variations likely marked the transition from O_2-deficient Proterozoic oceans to widely oxygenated later Phanerozoic oceans.

1. INTRODUCTION

High concentrations of environmental oxygen are a physiological requirement for the evolution of metabolically active metazoans capable of movement and predation (Towe, 1970; Runnegar, 1991; Knoll and Carroll, 1999; Knoll, 2011). The time when this requirement was met is not precisely known. Furthermore, there is debate about whether or not environmental oxygenation is the main driver of trends in early metazoan evolution, once the physiological requirement was met. Some studies highlight a direct connection between the initial diversification of Ediacaran metazoans and ocean oxygenation, for example, in the aftermath of the ca. 635 Ma end-Cryogenian glaciation (Planavsky et al., 2010; Sahoo et al., 2012). Alternatively, a significant time lag between the attainment of sufficient oxygen levels and the diversification of metazoans may have arisen from genetic and ecological factors (Erwin et al., 2011; Mills et al., 2014; Penny et al., 2014; Planavsky et al., 2014). The appearance of more

complex eukaryotes, including early metazoans, may have led to more extensive ocean oxygenation (Butterfield, 2009; Lenton et al., 2014). Environmental and ecological triggers may have acted in tandem to drive metazoan diversification, culminating in the Cambrian Explosion (Sperling et al., 2013a). Understanding the relationship between environmental oxygen levels and metazoan evolution ultimately requires higher resolution geochemical, geochronological, and biostratigraphic data, as well as improved quantitative constraints on spatiotemporal changes in atmosphere and ocean redox conditions (e.g., Och and Shields-Zhou, 2012; Lowenstein et al., 2014; Lyons et al., 2014).

Geochemical proxies for the extent of ocean oxygenation during the Ediacaran Period suggest a time of complicated redox changes. High concentrations of the redox-sensitive metals Mo and V are found in the earliest Ediacaran (ca. 632 Ma) organic-rich mudrocks (ORM) of the Doushantuo Formation (South China). The high Mo and V concentrations point to a larger oceanic Mo and V inventory as a result of increased deep ocean oxygenation (Sahoo et al., 2012). However, there is no compelling evidence for extensive oxygenation during the remainder of the early Ediacaran Period. For example, sedimentary Fe speciation, S and Fe isotope data, and low Mo concentrations in ORM suggest widely anoxic oceans containing low marine sulfate concentrations (Canfield et al., 2008; McFadden et al., 2008; Li et al., 2010; Fan et al., 2014; Guan et al., 2014). These data suggest that the oceans largely retained a Proterozoic-style, redox-stratified character during the early Ediacaran Period.

There is geochemical evidence to support episodes of late Ediacaran ocean oxygenation. Although sedimentary Fe speciation data continue to point to regions of at least locally anoxic deep oceans (Canfield et al., 2008; Li et al., 2010; Frei et al., 2013; Johnston et al., 2013), the same proxy suggests that parts of the deep ocean became oxygenated after the end of the ca. 580

Ma Gaskiers glaciation (Canfield et al., 2007, 2008; Johnston et al., 2012a). High Mo concentrations in ca. 560-551 Ma ORM of Member IV, upper Doushantuo Formation (South China), point to a more globally oxygenated state for the oceans (Scott et al., 2008; Li et al., 2010; Och and Shields-Zhou, 2012). However, the absence of evidence for late Ediacaran ocean oxygenation in some ocean basins has led some researchers to question the extent of oxygenation (Johnston et al., 2013). The isotopic compositions of U and Mo in anoxic and sulfidic (euxinic) ORM are a promising approach for constraining the global extent of ancient ocean oxygenation (Arnold et al., 2004; Weyer et al., 2008). Here, we present new U and Mo isotope data from Member IV ORM that provide further evidence for extensive ocean oxygenation ca. 560-551 Myr ago. We also present an updated Mo isotope compilation for ORM that suggests multiple transient episodes of widespread ocean oxygenation occurred at the Precambrian-Phanerozoic transition.

2. MEMBER IV, DOUSHANTUO FORMATION, SOUTH CHINA

The Doushantuo Formation was deposited between 635 and 551 Ma on a passive margin continental shelf (Nanhua Basin, South China) on the Yangtze Block following the breakup of Rodinia (Wang and Li, 2003; Jiang et al., 2003). The Doushantuo Formation is underlain by glacial diamictites of the Nantuo Formation, deposited during the widespread end-Cryogenian glaciation, and is overlain by carbonates of the latest Ediacaran Dengying Formation. In the Three Gorges region, located ~30 km west of Yichang (Fig. 1), the Doushantuo Formation was deposited on the inner shelf (Western Hubei Platform) below wave base (McFadden et al., 2008; Jiang et al., 2011). Here, the formation is up to 250 m thick and comprises a basal ~5 m thick

dolostone (Member I), interbedded ORM and dolostones containing abundant chert nodules (Member II), dolostone that passes into interbedded limestone and dolomitic mudstone (Member III), and a ~5-15 m thick interval of ORM (Member IV) (Fig. 2, Zhou and Xiao, 2007; McFadden et al., 2008; Sawaki et al., 2010; Jiang et al., 2011).

Fossil assemblages in the Doushantuo Formation and correlatives include macroscopic carbonaceous compressions of eukaryotes, multicellular algae, acanthomorph acritarchs, and possible animal eggs and embryos (Xiao et al., 2002; Yin et al., 2007; McFadden et al., 2008; Yuan et al., 2011; Schiffbauer et al., 2012; Chen et al., 2014). Alternative interpretations for these embryo-like fossils, such as non-metazoan holozoans (Huldtgren et al., 2011) or sulfur bacteria (Bailey et al., 2007), are inconsistent with their morphology, taphonomy and multicellularity (Xiao et al., 2007, 2012; Schiffbauer et al., 2012; Chen et al., 2014). The overlying carbonates of the latest Ediacaran Dengying Formation preserve macroscopic metazoan body fossils, biomineralizing metazoans (e.g., *Cloudina* and *Sinotubulites*), and large horizontal trace fossils made by motile bilaterians (Xiao et al., 2005; Weber et al., 2007; Chen et al., 2008).

To obtain better quantitative constraints on the extent of late Ediacaran ocean oxygenation, we measured U and Mo isotope compositions, Fe speciation, and total organic carbon (TOC) concentrations for the Member IV ORM. Our measurements were obtained from the well-studied Jiulongwan outcrop section, Three Gorges region (McFadden et al., 2008), plus a recently drilled core collected 5 km farther southwest (Site 1 of Sawaki et al., 2010) to test lateral homogeneity of the data and to verify that deleterious oxidative weathering was negligible. Previous work has revealed high Mo concentrations in Member IV, which most likely requires a large dissolved Mo reservoir, suggesting both significant ocean oxygenation and a

good connection between the Nanhua Basin and open ocean (Scott et al., 2008; Sahoo et al., 2012).

Precise absolute age constraints for the duration of Member IV deposition have been challenging to obtain. The end of Member IV deposition is well-constrained by a U-Pb zircon age of 551.1 ± 0.6 Ma (Mean Square of Weighted Deviates [MSWD] = 0.48) from an ash bed nearly 1 m below the top of the member (from the Jiuqunao section located ~20 km northwest of the Three Gorges region; Condon et al., 2005). However, the onset of Member IV deposition is poorly constrained. The top of Member IV (ca. 551 Ma) marks the end of a prominent negative $\delta^{13}C$ excursion that began in Member III (Jiang et al., 2007; Zhou and Xiao, 2007; Zhu et al., 2007; McFadden et al., 2008; Sawaki et al., 2010). This excursion has been correlated with the Shuram $\delta^{13}C$ excursion in Oman (Fike et al., 2006; Le Guerroué, 2010), the Wonoka $\delta^{13}C$ excursion in Australia (Calver, 2000; Retallack et al., 2014), and the Krol B $\delta^{13}C$ excursion in India (Kaufman et al., 2006; Jiang et al., 2007). Although there is no absolute age constraint for the duration of this $\delta^{13}C$ excursion in any of these successions, stratigraphic analyses and Sr isotope data suggest that the Doushantuo-Shuram-Wonoka-Krol isotope anomaly is younger than the Gaskiers glaciation (Calver, 2000; Fike et al., 2006; Le Guerroué, 2010; Sawaki et al., 2010). This interpretation is in line with the suggestion that the stratigraphic break at the Member II-III transition reflects sea-level fall during the Gaskiers glaciation and is thus ca. 580 Ma (Condon et al., 2005; Tahata et al., 2013). Considering that the Doushantuo Formation (ca. 635–551 Ma) covers ~90% of Ediacaran time, a simple age extrapolation would place the base of Member IV at ca. 560 Ma (e.g., Jiang et al., 2007). This estimate is consistent with a Pb-Pb age of 576 ± 14 Ma (MSWD = 0.4) from the upper phosphorite layers (Member III correlative) of the Doushantuo Formation in Weng'an, located 750 km to the southwest of the Three Gorges region

(Chen et al., 2004), and the similarity of acritarch fossils between the Jiulongwan and Weng'an sections (e.g., Zhou et al., 2007; Xiao et al., 2014).

Recently, a Re-Os age of 595 ± 22 Ma (MSWD = 29) was reported from ORM at the base of Member IV in the Jiulongwan section (Zhu et al., 2013). A more precise Re-Os age of 591.1 ± 5.3 Ma (MSWD = 1.3) was derived from a subset of four analyses that made up the 7-point Re-Os isochron regression of 595 ± 22 Ma. Zhu et al. (2013) attributed the excess scatter in the 7-point regression to initial $^{187}Os/^{188}Os$ heterogeneity (i.e., variations in seawater $^{187}Os/^{188}Os$) rather than post-depositional disturbance. However, the seven samples were obtained from a lateral interval of only ~5 to 10 cm thick, raising doubts about whether variations in seawater $^{187}Os/^{188}Os$ can explain the high MSWD. As discussed below, the basal Member IV ORM from the Jiulongwan section have unusual Mo and U isotope signatures, which may reflect post-depositional modification that could have had an adverse effect on the Re-Os age of Zhu et al. (2013). In addition, the Re-Os age of ca. 591 Ma implies that the ≤ 10-m-thick Member IV black shales span 40 Myr of time. This is unlikely unless a major unconformity or hiatus is found within Member IV in future studies. Therefore, we prefer to estimate the age of Member IV as ca. 560–551 Ma.

3. ANALYTICAL METHODS

3.1 Uranium isotopes

All U and Mo isotope data were obtained at the W. M. Keck Foundation Laboratory for Environmental Biogeochemistry, School of Earth and Space Exploration, Arizona State University. Uranium isotope measurements were made following the protocols outlined in

Weyer et al. (2008) and Kendall et al. (2013). Powdered sample splits (75-100 mg) were ashed overnight at 550°C and dissolved completely by HF-HNO_3-HCl acid digestion. A split of the sample solution was diluted with 2% HNO_3 and analyzed for U concentrations on a Thermo Scientific X series quadrupole ICP-MS (inductively coupled plasma mass spectrometer). Instrument accuracy was verified using secondary standard solutions, including the USGS Devonian black shale standard SDO-1. Analyte concentration reproducibility was within 5%.

Uranium isotope compositions were measured on a Thermo Scientific Neptune multi-collector ICP-MS using a ^{236}U:^{233}U double spike (IRMM-3636; Verbruggen et al., 2008) to correct for instrumental mass bias. The spike was equilibrated with sample solutions, and U was subsequently isolated from the sample-spike mixture using Eichrom® UTEVA resin. Sample $\delta^{238}U$ is reported as per mil deviations from the CRM145 standard [$\delta^{238}U = (^{238/235}U_{sample}/^{238/235}U_{standard} - 1) \times 1000$]. Repeated measurements of the U isotope standards SRM950a and CRM129a yielded average $\delta^{238}U$ values of 0.04 ± 0.06 ‰ (2SD; n = 38) and –1.72 ± 0.09 ‰ (2SD; n = 124), respectively. Hence, U isotope data reported relative to CRM145 are statistically identical to U isotope data reported relative to SRM950a (e.g., Weyer et al., 2008; Montoya-Pino et al., 2010; Brennecka et al., 2011a, b; Kendall et al., 2013). We also measured four full powder replicates of SDO-1 during the course of this study, and these analyses gave an average of –0.06 ± 0.04 ‰ (2SD; n = 17). We report the 2SD uncertainty of a sample as the 2SD uncertainty of sample replicate measurements or 0.07 ‰ (average of the uncertainties given above for SRM950a, CRM129a, and SDO-1), whichever is greater.

3.2 Molybdenum isotopes

Molybdenum concentration and isotope data were obtained following the methods outlined in Kendall et al. (2009a) and Duan et al. (2010). After sample dissolution using the methods outlined above, samples were purified for Mo using anion and cation exchange chromatography. For each sample, Mo concentrations were measured before and after chromatography to verify that column yields were >95%. For optimal precision of column yield measurements, Mo concentrations were determined by isotope dilution quadrupole ICP-MS, and all of the digested sample solution was used for column chemistry (hence, separate splits of the sample powders were used for Mo and U isotope measurements). The Mo isotope compositions were measured by multi-collector ICP-MS using sample-standard bracketing and a Zr element spike (prepared from Johnson Matthey Specpure® Zr plasma standard solution; Lot #700193E) to correct for instrumental mass fractionation (these measurements were done before implementation of the Mo double spike technique at Arizona State University). Our Mo isotope data were originally measured relative to the Johnson Matthey Specpure® Mo plasma standard (Lot #802309E; RochMo2).

Sample δ^{98}Mo was re-calculated as per mil deviations from the new international NIST SRM 3134 standard as follows: $\delta^{98}Mo = [{}^{98/95}Mo_{sample}/({}^{98/95}Mo_{standard} * 0.99975) - 1] \times 1000$ (Goldberg et al., 2013; Nägler et al., 2014). The logic behind setting the NIST SRM 3134 standard to 0.25‰ (instead of 0‰) is to retain comparison of sample δ^{98}Mo data with the "traditional" seawater δ^{98}Mo value of 2.3‰ (Nägler et al., 2014). On this scale, seawater has a value of 2.34 ± 0.10 ‰, and RochMo2 has a value of –0.08 ± 0.05 ‰ (Goldberg et al., 2013; Nägler et al., 2014). For an eighteen month period covering the Mo isotope analyses in this study, the average δ^{98}Mo for SDO-1, based on five separate powder digestions, was 0.83 ± 0.15

‰ relative to NIST SRM 3134 = 0‰ or 1.08 ± 0.15 ‰ relative to NIST SRM 3134 = 0.25‰ (2SD, n=238). The first value is in excellent agreement with the SDO-1 average of 0.80 ± 0.14 ‰ reported by Goldberg et al. (2013). Given the average uncertainty of SDO-1, we report the 2SD uncertainty of a sample as the 2SD uncertainty of sample replicate measurements or 0.15 ‰, whichever is greater.

3.3 Sedimentary iron speciation

Preservation of seawater δ^{98}Mo is most likely to occur in ORM deposited beneath strongly euxinic bottom waters (Barling et al., 2001; Arnold et al., 2004; Neubert et al., 2008; Gordon et al., 2009). Hence, sedimentary Fe speciation was used to reconstruct local bottom water redox conditions at the studied localities. Transport, scavenging, and enrichment of Fe occur in modern anoxic marine basins. The sediments accumulating in such settings have ratios of biogeochemically highly reactive Fe (Fe_{HR}) to total Fe (Fe_T) that are higher (typically >0.38) compared to modern sediments (0.26 ± 0.08) and Phanerozoic sedimentary rocks (0.14 ± 0.08) deposited from oxygenated bottom waters (Raiswell and Canfield, 1998; Poulton and Raiswell, 2002; Lyons and Severmann, 2006). Biogeochemically highly reactive Fe (Fe_{HR}) is defined as pyrite Fe (Fe_{PY}) and other Fe phases (carbonates [Fe_{Carb}], ferric oxides [Fe_{Ox}], and mixed-valence Fe oxides, primarily magnetite [Fe_{Mag}]) that will react with sulfide in the water column or in sediments during early diagenesis. Hence, $Fe_{HR} = Fe_{PY} + Fe_{Carb} + Fe_{Ox} + Fe_{Mag}$ (Poulton et al., 2004; Poulton and Canfield, 2005). The modern baseline for Fe_{HR}/Fe_T was derived using $Fe_{HR} = Fe_{PY}$ (pyrite) + Fe_{Ox} (ferric oxides) (Raiswell and Canfield, 1998). Although Fe_{HR} has been expanded to include Fe_{Carb} (carbonates) and Fe_{Mag} (mixed-valence Fe oxides) because of their importance in ancient ORM (Poulton et al., 2004; Poulton and Canfield, 2005), comparison with

231 the modern baseline is still justified given the scarcity of Fe_{Carb} and Fe_{Mag} in modern sediments.
232 The extent to which Fe_{HR} has been converted to pyrite (Fe_{PY}) is used to determine if the bottom
233 waters were euxinic ($Fe_{PY}/Fe_{HR} > 0.7$) or ferruginous ($Fe_{PY}/Fe_{HR} < 0.7$) (some studies use the
234 older boundary value of 0.8; Anderson and Raiswell, 2004; Poulton et al., 2004; Poulton and
235 Canfield, 2011).

236 Sedimentary Fe speciation analyses were carried out at the University of California,
237 Riverside. A sequential extraction method (Poulton and Canfield, 2005), followed by analysis on
238 an Agilent 7500ce ICP-MS, was used to determine Fe_{Carb} + Fe_{Ox} + Fe_{Mag} (Li et al., 2010).
239 Analytical reproducibility was typically within 5%, with the exception of some low-Fe samples
240 (<0.1 wt%). Pyrite Fe was determined from the weight percent of S extracted during a 2-hour
241 chromium chloride distillation, assuming a stoichiometry of FeS_2.

242

243 **3.4 Total organic carbon**

244 Measurements of total organic carbon (TOC) were made at the Japan Agency of Marine-
245 Earth Science and Technology (JAMSTEC) and are described in Kikumoto et al. (2014). A
246 known amount of powdered sample was first demineralized by 10 M HCl at 70°C for >24 hours.
247 Residues were rinsed with pure water and ethanol, dried, weighed, and combusted at 1000°C
248 with an elemental analyzer (EA) connected to a Finnigan Delta XP mass spectrometer.
249 Abundances of the resultant CO_2 gas were measured by a conventional EA-IRMS method.
250 Additional TOC measurements, derived from the difference between total carbon (determined by
251 combustion) and total inorganic carbon (determined by acidification), were made using an Eltra
252 CS-500 carbon/sulfur analyzer at the University of California, Riverside, as described in Scott et

al. (2008) and Li et al. (2010). For both methods, the analytical reproducibility of TOC contents is 0.10 wt% or better based on repeated analyses of standards.

4. RESULTS

4.1 Sedimentary iron speciation and metal concentrations

All samples from the Jiulongwan outcrop section and the Site 1 drill core section have $Fe_{HR}/Fe_T > 0.38$ and $Fe_{PY}/Fe_{HR} > 0.7$, indicating that the inner shelf was persistently covered by euxinic bottom waters during deposition of Member IV, consistent with prior data (Table 1 and Fig. 2; Scott et al., 2008; Li et al., 2010). This interpretation is further supported by high Mo concentrations (25-663 ppm; average = 138 ppm) and U concentrations (5-97 ppm; average = 22 ppm) in the Member IV ORM (Tribovillard et al., 2006; Scott and Lyons, 2012).

To further establish local depositional conditions in the Nanhua Basin during Member IV time, we compared the enrichment factors (EFs) of Mo and U relative to average upper crust. The EF is calculated as follows (Tribovillard et al., 2006):

$$EF_{\text{element X}} = (X/Al)_{\text{sample}} / (X/Al)_{\text{average upper crust}}$$

Average upper crust concentrations are Mo = 1.5 ppm, U = 2.8 ppm, and Al = 80,400 ppm (McLennan, 2001). High EF values for both Mo (35-512; average = 142) and U (5-52; average = 14) indicate a dominance of hydrogenous over detrital contributions of Mo and U to Member IV ORM. The Mo/U ratios of Member IV ORM consistently exceed those of modern seawater (Fig. 3a). This observation is consistent with the occurrence of locally euxinic bottom waters, and unrestricted exchange between the local depositional basin and the open ocean (Algeo and Tribovillard, 2009). High Mo/U ratios in ORM can also be caused by the operation of a

particulate Fe-Mn oxyhydroxide shuttle in a weakly restricted basin (as in the modern Cariaco Basin), which leads to more efficient removal of Mo from the water column to sediments compared to U (Algeo and Tribovillard, 2009).

4.2 Uranium and molybdenum isotope compositions

The U and Mo isotope data were not corrected for detrital contributions because of the dominance of hydrogenous over detrital U and Mo in the Member IV ORM. Despite the persistence of euxinic bottom waters at the studied localities, the stratigraphic trends of $\delta^{238}U$ and $\delta^{98}Mo$ are significantly different (Fig. 2), with no significant correlation between them (Fig. 3b). In the Jiulongwan outcrop section, a few samples (HND 30.35, HND 29.5, HND 28.85) at the base of Member IV have the lowest $\delta^{98}Mo$ (–1.3 to –0.5 ‰) and highest $\delta^{238}U$ (0.4-0.5‰). The rest of Member IV in the Jiulongwan section has uniform $\delta^{238}U$ (0.2-0.4‰) except for one outlier near the top of the section (sample HN-23 = –0.4‰). In contrast, the Mo isotope data show a more complex pattern. The exceptionally low $\delta^{98}Mo$ at the base gives way upsection to $\delta^{98}Mo$ values between –0.4‰ and +0.4‰. This trend is followed up section by an excursion to high $\delta^{98}Mo$ (up to 2.0 ‰) near the top of Member IV. A return to low $\delta^{98}Mo$ values marks the top of Member IV.

Stratigraphic trends in the Site 1 drill core section are similar to the Jiulongwan section except for the absence of exceptionally low $\delta^{98}Mo$ and exceptionally high $\delta^{238}U$ at the base of Member IV. Hence, these few unusual isotopic signatures at the base of the Jiulongwan section are possible post-depositional artifacts (e.g., modification by surficial fluids concentrated along the Member III-IV contact) and are not considered further. In the Site 1 drill core, there is minimal variation in $\delta^{238}U$ (0.1-0.3 ‰) except for one outlier at the top of the section (sample

40-4-of-12 = –0.13‰). The δ^{98}Mo of lower Member IV ranges between –0.5‰ and +0.2‰. As in the Jiulongwan section, there is an excursion to high δ^{98}Mo (up to 1.7 ‰) near the top of Member IV, which is followed by a return to lower δ^{98}Mo.

Hence, there are two major observations from the isotopic data: (1) dominantly uniform δ^{238}U throughout most of Member IV (average δ^{238}U = 0.24 ± 0.16 ‰, 2SD, 34 out of 39 samples; excluding HN-23, HND 30.35, HND 29.5, HND 28.85, and 40-4-of-12) and (2) a prevalence of δ^{98}Mo values near 0‰ in Member IV except for an excursion to high δ^{98}Mo (1.7-2.0 ‰) near the top of both sections.

5. DISCUSSION

5.1 Uranium isotopes: evidence for widespread ocean oxygenation at ca. 560-551 Ma

Recent advances in our understanding of the modern marine U isotope budget have led to the application of U isotope data from ORM and carbonates as a paleoredox proxy (Weyer et al., 2008; Montoya-Pino et al., 2010; Brennecka et al., 2011a; Asael et al., 2013; Kendall et al., 2013; Andersen et al., 2014; Dahl et al., 2014). In oxygenated seawater, uranium exists as dissolved U(VI), primarily as the uranyl carbonate anion ($UO_2[CO_3]_3^{4-}$; Langmuir, 1978), and has a conservative distribution in the oceans with a residence time of ~400-500 kyr (Ku et al., 1977; Dunk et al., 2002). The single major source of U to the oceans is oxidative mobilization of U from the upper continental crust and transport of dissolved U(VI) to the oceans via rivers (Dunk et al., 2002). In contrast, there are multiple marine sinks for U. Biogenic carbonates, sediments deposited beneath anoxic bottom waters, and sediments deposited beneath weakly oxygenated bottom waters are major sinks. Minor sinks include sediments deposited beneath

well-oxygenated bottom waters and the hydrothermal alteration of oceanic crust (Morford and Emerson, 1999; Dunk et al., 2002; Partin et al., 2013).

In anoxic basins, U is primarily removed below the sediment water-interface rather than in the water column (Anderson et al., 1989; Barnes and Cochran, 1990). Uranium can be precipitated from sediment pore waters as UO_2 or adsorbed to organic matter following the reduction of dissolved U(VI) to U(IV) at the depth of microbial Fe^{3+} and SO_4^{2-} reduction (see recent reviews on U marine geochemistry by Algeo and Tribovillard, 2009; Asael et al., 2013; Partin et al., 2013). The reduction and removal of U to the euxinic sediments of the deep Black Sea is accompanied by a large volume-dependent equilibrium isotope fractionation that favors the removal of heavier U isotopes from the water column (Schauble, 2006; Weyer et al., 2008; Montoya-Pino et al., 2010; Andersen et al., 2014). Taking the offset between the average $\delta^{238}U$ of recent Unit I organic-rich sediments deposited from strongly euxinic waters at water depths of >2000 m (0.02 ± 0.12 ‰) and modern seawater (–0.40 ± 0.03 ‰), the magnitude of isotope fractionation is ~0.4 ‰ (Weyer et al., 2008; Andersen et al., 2014). A similar offset was determined between Unit I sediments and seawater at a water depth of 418 m (Weyer et al., 2008; Montoya-Pino et al., 2010). Given the restricted setting of the Black Sea, with ~40% U depletion in the deep euxinic water column (Anderson et al., 1989), the observed offset between Unit I sediments and seawater is only a minimum for open ocean settings. Using mass balance modeling, Andersen et al. (2014) suggest that in an open ocean setting characterized by strong U recharge to locally euxinic bottom waters and U removal from solution below the sediment-water interface, the U isotope fractionation between euxinic sediments and modern seawater will be ~0.6‰, which corresponds to a euxinic sediment $\delta^{238}U$ of ~0.2‰.

In contrast to the anoxic sink, the other marine sinks are associated with small U isotope fractionations. Peruvian continental margin sediments underlying weakly oxygenated waters have an average $\delta^{238}U$ of –0.28 ± 0.19 ‰, which is only ~0.1 ‰ higher than seawater (Weyer et al., 2008). The surface layers of Fe-Mn crusts in sediments underlying well-oxygenated bottom waters (–0.65 ± 0.05 ‰) show an opposite sense of isotope fractionation and have $\delta^{238}U$ that is ~0.24 ‰ lower than seawater (Weyer et al., 2008; Brennecka et al., 2011b; Goto et al., 2014). The U isotope fractionation accompanying hydrothermal alteration of oceanic crust may be minimal if fresh and altered basalts typically have similar $\delta^{238}U$ (Noordmann et al., 2010, 2011). Primary biological and abiological carbonate precipitates show negligible offset from seawater (Stirling et al., 2007; Weyer et al., 2008; Romaniello et al., 2013; Andersen et al., 2014). An exception is shallow-water carbonate sediments containing dissolved sulfide in pore waters, which can have $\delta^{238}U$ values of 0.2-0.4 ‰ higher compared to seawater (Romaniello et al., 2013).

Well-oxygenated bottom waters dominate the modern ocean. Because the expression of U isotope fractionation in oxygenated sediments is small, and the areal extent of weakly oxygenated to anoxic bottom waters is limited, the $\delta^{238}U$ of seawater is only slightly lower compared to riverine inputs (–0.3 to 0.0 ‰; Stirling et al., 2007; Noordmann et al., 2010, 2011). In contrast, at times of expanded ocean anoxia, seawater $\delta^{238}U$ will be lower because of extensive preferential removal of isotopically heavy U isotopes to euxinic sediments (Weyer et al., 2008; Montoya-Pino et al., 2010; Brennecka et al., 2011a). Hence, expanded ocean anoxia should cause the $\delta^{238}U$ of ancient euxinic ORM deposited in an open ocean euxinic setting to be lower than ~0.2‰ (Andersen et al., 2014).

366 Using this modern framework, we interpret the high average $\delta^{238}U$ of 0.24 ± 0.16 ‰ for
367 most Member IV ORM as evidence for widespread ocean oxygenation ca. 560-551 Myr ago. The
368 average $\delta^{238}U$ value from Member IV is similar to the predicted $\delta^{238}U$ for a hypothetical modern
369 euxinic sediment deposited in an unrestricted ocean basin. High Mo/U and Mo/TOC ratios for
370 Member IV ORM indicate that water exchange between the local depositional environment and
371 the open ocean was not severely restricted (Algeo and Lyons, 2006; Algeo and Tribovillard,
372 2009). The average Mo/TOC ratio of 23 ppm/wt% for Member IV ORM (excluding the three
373 samples from the base of the Jiulongwan section) is similar to the average of 25 ppm/wt% for the
374 weakly restricted Cariaco Basin (Algeo and Lyons, 2006). Hence, we suggest that the U isotope
375 fractionation between the Member IV euxinic sediments and global seawater was close to 0.6 ‰,
376 thus implying a late Ediacaran seawater $\delta^{238}U$ that was near the modern seawater value of –
377 0.4‰. Our interpretation assumes that riverine $\delta^{238}U$ during late Ediacaran time was broadly
378 similar to modern values of –0.3 to 0.0 ‰. However, Ediacaran rivers may have lower $\delta^{238}U$
379 compared to modern rivers because Precambrian ORM with both high U concentrations and high
380 $\delta^{238}U$, a signature of well-oxygenated oceans, were probably less available for weathering (Partin
381 et al., 2013). A lower riverine $\delta^{238}U$ implies that the seawater $\delta^{238}U$ of a well-oxygenated
382 Ediacaran ocean was lower than modern seawater. Hence, the high average $\delta^{238}U$ of euxinic
383 Member IV ORM suggests extensive ocean oxygenation on a scale similar to or even greater
384 than today.

385 Our interpretation is consistent with high Mo concentrations in Member IV ORM, which
386 point to a high seawater Mo inventory in well-oxygenated oceans (Scott et al., 2008), and Fe
387 speciation evidence for locally oxygenated deep waters in some late Ediacaran ocean basins

(Canfield et al., 2008; Johnston et al., 2012). Solitary low $\delta^{238}U$ values at the top of both sections may suggest a transient episode of expanded ocean anoxia during Member IV time.

The development of locally anoxic basins in continental margin environments is not precluded by our data and thus is not incompatible with geochemical evidence for local anoxia in some late Ediacaran sedimentary basins (e.g., Canfield et al., 2008; Frei et al., 2013; Johnston et al., 2013). However, our data do indicate that anoxia was comparatively minor relative to ocean oxygenation at ca. 560-551 Ma. Our interpretations are based on the concentration and isotopic composition of redox-sensitive trace metals (Mo, U) with long oceanic residence times (400-500 kyr). These geochemical tools, when applied to euxinic ORM, are more favorable for constraining the global extent of ocean oxygenation and anoxia (Arnold et al., 2004; Weyer et al., 2008) compared to elements with short oceanic residence times.

Extensive ocean oxygenation ca. 560-551 Myr ago is coincident with the later stages of the Shuram negative carbon isotope excursion (Fig. 4). In South China, the onset of the Shuram excursion occurs in Member III and ends at the Doushantuo-Dengying transition (Jiang et al., 2007; Zhou and Xiao, 2007; Zhu et al., 2007; McFadden et al., 2008; Sawaki et al., 2010; Tahata et al., 2013). Because U isotope data are not available for Member III, we cannot determine if widespread ocean oxygenation occurred during the entirety of the Shuram excursion. Hence, we consider it beyond the scope of this paper to delve into the debate surrounding the origin of the Shuram excursion (Grotzinger et al., 2011).

5.2 Molybdenum isotopes: Constraints on global and local ocean redox conditions

Molybdenum is oxidatively mobilized from the upper continental crust beneath an oxygenated atmosphere and is transported to the oceans primarily by rivers as largely unreactive

411 MoO_4^{2-} (molybdate). Molybdenum behaves conservatively in oxygenated seawater and thus
412 accumulates in the oceans, leading to a long oceanic residence time of ~440 kyr (Miller et al.,
413 2011). Upon encountering sulfidic conditions in the water column or sediment pore fluids,
414 MoO_4^{2-} is converted to $MoO_{4-x}S_x^{2-}$ (thiomolybdate) (Helz et al., 1996; Erickson and Helz, 2000)
415 and then, at least in some settings, to reactive Mo-polysulfide species (Dahl et al., 2013). These
416 species are then scavenged by Fe sulfide minerals (Helz et al., 1996, 2004) and organic particles
417 (Helz et al., 1996; Tribovillard et al., 2004; Chappaz et al., 2014) or undergo equilibrium
418 precipitation as a Fe(II)-Mo(VI) sulfide mineral (Helz et al., 2011), thus removing Mo to
419 sediments.

420 Where marine bottom waters become highly sulfidic ("strongly euxinic"; $[H_2S]_{aq}$ >11
421 μM), the quantitative conversion of MoO_4^{2-} to MoS_4^{2-} (tetrathiomolybdate) and its removal from
422 bottom waters can lead to the preservation of seawater δ^{98}Mo in sediments (Barling et al., 2001;
423 Arnold et al., 2004; Neubert et al., 2008). Doubts have been raised as to whether quantitative Mo
424 removal is characteristic of highly sulfidic marine basins (Helz et al., 2011). However, a small
425 isotopic offset between dissolved MoS_4^{2-} and authigenic solid Mo (Δ^{98}Mo ~0.5 ± 0.3‰; Nägler
426 et al., 2011) suggests the δ^{98}Mo of strongly euxinic sediments will closely approximate seawater
427 even if Mo removal from bottom waters is not quantitative. The long seawater Mo residence time
428 means that the δ^{98}Mo of strongly euxinic sediments at a single locality, including basins with
429 semi-restricted access to the open ocean, can stand as a proxy for global seawater, as shown for
430 the modern Black Sea (Barling et al., 2001; Arnold et al., 2004; Neubert et al., 2008).

431 Seawater δ^{98}Mo represents an ocean redox proxy because it records the relative
432 proportion of Mo buried in marine sediments deposited beneath O_2-rich and O_2-poor waters.
433 Global seawater today is enriched in heavy Mo isotopes (δ^{98}Mo = 2.34 ± 0.10‰; Barling et al.,

2001; Siebert et al., 2003; Nakagawa et al., 2012; Nägler et al., 2014) relative to oceanic inputs (dominated by rivers, average δ^{98}Mo ~0.7‰; Archer and Vance, 2008). The extent of this enrichment results largely from the preferential adsorption of light Mo isotopes in seawater onto Mn oxides in sediments beneath oxygenated waters. The isotope fractionation during this process is large (~3‰; Barling et al., 2001; Siebert et al., 2003, Barling and Anbar, 2004; Wasylenki et al., 2008; Poulson Brucker et al., 2009). In contrast, isotope fractionation is often smaller (typically ≤1‰) during Mo burial in low-O_2 (<10 µM) and anoxic marine environments where H_2S is present in pore and/or bottom waters (Barling et al., 2001; Arnold et al., 2004; Poulson et al., 2006; Siebert et al., 2006; Neubert et al., 2008; Poulson Brucker et al., 2009). A notable exception is weakly euxinic environments ($[H_2S]_{aq}$ <11 µM) where sediments have δ^{98}Mo that is up to 3.0‰ lower than seawater because of the incomplete conversion of molybdate to tetrathiomolybdate and the preservation of Mo isotope fractionation during the formation of intermediate thiomolybdate complexes (Arnold et al., 2004, 2012; Neubert et al., 2008; Dahl et al., 2010a; Nägler et al., 2011; Azrieli-Tal et al., 2014). In continental margin environments where bottom waters are mildly oxygenated (e.g., 10-35 µM) and sediments are characterized by active Fe-Mn oxide recycling above a deeper zone of dissolved sulfide, sediments have δ^{98}Mo that is intermediate between the well-oxygenated and strongly euxinic end-members (Siebert et al., 2006; Poulson Brucker et al., 2009; Goldberg et al., 2012). The general picture that emerges is that high seawater δ^{98}Mo reflects well-oxygenated oceans whereas low seawater δ^{98}Mo points to extensive ocean anoxia, specifically a greater extent of strongly euxinic waters because it is in such environments that Mo isotope fractionation between seawater and sediment is smallest. In this way, the δ^{98}Mo of ancient seawater, as inferred from euxinic ORM, can be used to elucidate

456 past global ocean redox conditions (e.g., Arnold et al., 2004; Dahl et al., 2010b; Kendall et al.,
457 2011).

458 High δ^{98}Mo values (1.7-2.0‰) near the top of Member IV in both sections approach the
459 modern seawater value of 2.3‰, which points to widespread oxygenation of the oceans just prior
460 to 551 Ma (Fig. 1). The highest δ^{98}Mo in Member IV represents a minimum value for seawater
461 because of the possibility of isotopic fractionation between dissolved MoS_4^{2-} and authigenic solid
462 Mo, which results in preferential removal of light Mo isotopes to sediments.

463 Seawater δ^{98}Mo is determined by the isotopic composition of inputs to the ocean and the
464 relative proportion of Mo buried into sediments of different redox character. The δ^{98}Mo of the
465 upper continental crust and riverine inputs is suggested to be broadly uniform during the past 2.7
466 Ga because no correlation exists between δ^{98}Mo and age for molybdenites, a major source of
467 oceanic Mo (Hannah et al., 2007). Nevertheless, Ediacaran rivers could have had lower δ^{98}Mo
468 than modern rivers because ORM with both high Mo concentrations and high δ^{98}Mo, indicative
469 of well-oxygenated conditions, were probably less available for weathering compared to today
470 (see section 5.3). Hence, an Ediacaran seawater δ^{98}Mo of ≥2.0 ‰ suggests that the ratio of
471 dissolved Mo buried in mildly/strongly oxygenated versus low-O_2/anoxic marine environments
472 was comparable to or higher than that observed in today's predominantly oxygenated oceans.

473 In the isotopically heavy part of Member IV, the Mo/TOC ratios, which scale with Mo
474 concentrations in sulfidic bottom waters (Algeo and Lyons, 2006), reach 32-34 ppm/wt%. These
475 ratios are similar to those of Phanerozoic euxinic ORM, reflecting enrichment under a large
476 dissolved Mo inventory and an appreciable extent of deep-ocean oxygenation (Scott et al., 2008;
477 Dahl et al., 2011; Dickson and Cohen, 2012; Sahoo et al., 2012; Reinhard et al., 2013). High

478 δ^{98}Mo signatures together with high Mo/TOC provide a compelling case for widespread ocean
479 oxygenation.

480 Alternative scenarios to explain the combination of high δ^{98}Mo and high Mo/TOC are
481 unlikely. Large isotopic offsets of up to ~3‰ lower than seawater are observed in modern Black
482 Sea sediments deposited beneath weakly euxinic waters near the chemocline ($[H_2S]_{aq}$ <11 μM;
483 Neubert et al., 2008). If weakly euxinic waters were widespread throughout the late Ediacaran
484 oceans and such environments were typically characterized by a Mo isotope fractionation of
485 ~3‰ between seawater and ORM, then the seawater δ^{98}Mo could have been driven to high
486 values. However, this scenario is challenged by the well-known observation that Mo burial
487 fluxes to sediments are ~2-3 orders of magnitude higher in the presence of H_2S relative to O_2,
488 even when dissolved H_2S in bottom waters is low (because sulfide is also present in sediment
489 pore waters; Scott et al., 2008; Poulson Brucker et al., 2009). The consequence of these high
490 burial rates is that the oceanic Mo inventory is sensitive to small changes in the extent of seafloor
491 covered by euxinic waters (Arnold et al., 2004). Recent modeling of the oceanic Mo inventory
492 and isotope mass balance demonstrates that if euxinia expanded to cover only 1% of the ocean
493 floor (compared to <0.1% today), then the seawater Mo concentration would be less than one-
494 third the modern value, and the Mo abundances and Mo/TOC ratios of euxinic ORM would be
495 low (Scott et al., 2008; Dahl et al., 2011; Sahoo et al., 2012; Reinhard et al., 2013). Hence,
496 widespread weakly euxinic oceans will not generate both high Mo/TOC and high δ^{98}Mo in
497 ORM.

498 Interpretation of the Mo isotope data from the stratigraphically underlying and overlying
499 ORM in Member IV is less straightforward. At face value, the low δ^{98}Mo (typically <0.8‰) of
500 these ORM suggests that seawater was isotopically light and hence that extensive Mo removal

occurred beneath anoxic (and especially euxinic) water masses. However, this interpretation conflicts with the high $\delta^{238}U$ and high Mo/TOC that point to extensive oxygenation (this study; Scott et al., 2008). Furthermore, some of these $\delta^{98}Mo$ values are appreciably lower than the modern oceanic input (~0.7‰). There is no known sink that can preferentially remove heavy Mo isotopes from seawater, so seawater $\delta^{98}Mo$ is unlikely to be lower than the oceanic input.

On this basis, we infer that the low $\delta^{98}Mo$ values are fractionated from coeval seawater. Sedimentary Fe speciation data point to persistently euxinic waters at the studied localities but do not reveal if bottom water sulfide concentrations were high enough for quantitative MoS_4^{2-} formation and the capture of seawater-like $\delta^{98}Mo$ in sediments. Following the Black Sea and Mediterranean examples (Neubert et al., 2008; Arnold et al., 2012; Azrieli-Tal et al., 2014), the lower $\delta^{98}Mo$ in Member IV ORM may record local deposition from weakly sulfidic waters and the associated expression of Mo isotope fractionation during formation of intermediate thiomolybdate complexes. In contrast, the higher $\delta^{98}Mo$ points to more intensely sulfidic local conditions. The high Mo/U ratios of Member IV ORM consistently exceed the modern seawater value, indicating that Mo was more efficiently transferred to the sediments compared to U (cf. Algeo and Tribovillard, 2009). Hence, it is possible that the prevalence of lower $\delta^{98}Mo$ reflects the operation of a particulate Fe-Mn oxyhydroxide shuttle analogous to that observed in the weakly euxinic Cariaco Basin (Algeo and Tribovillard, 2009). The Fe-Mn oxyhydroxide particles form at the chemocline where upwelling Fe^{2+} and Mn^{2+} comes into contact with oxygenated waters. These particles will preferentially adsorb the lighter isotopes of Mo while sinking through the water column. Reductive dissolution of Fe-Mn oxyhydroxide particles below the sediment-water interface releases Mo, which can then be sequestered by Fe sulfide minerals and organic particles, thus preserving a low $\delta^{98}Mo$ signature in sulfidic sediments (Herrmann et

al., 2012; Scholz et al., 2013). In both sections, the samples with highest δ^{98}Mo have among the lowest Mo/U ratios (see Fig. 3a), suggesting a decreased shuttle effect, along with increased bottom water sulfide concentrations, enabled better capture of seawater δ^{98}Mo in these samples.

5.3 Temporal trends in ocean oxygenation: the molybdenum isotope perspective

To explore the relevance of our data within a broader temporal context, we compiled δ^{98}Mo and associated Mo/TOC data from ORM deposited since the end of the Great Oxidation Event (Fig. 4; inadequate U isotope data exist for this purpose). We have recalculated the literature δ^{98}Mo values relative to NIST SRM 3134 as $\delta^{98}Mo = [(^{98/95}Mo_{sample}/(^{98/95}Mo_{standard} * 0.99975)) - 1] \times 1000$, following Nägler et al. (2014) by using the conversion values in Goldberg et al. (2013). Our compilation, updated from Dahl et al. (2010b), includes our new data from Member IV plus new data from the 640.7 ± 4.7 Ma Black River Dolomite (Kendall et al., 2009b; the Black River Dolomite is described in Appendix A and the data are reported in Table A.1). The compilation specifically targeted ORM deposited beneath euxinic bottom waters as defined by sedimentary Fe speciation (including degree-of-pyritization; Lyons and Severmann, 2006; Scott et al., 2008) and included intervals containing ORM with Mo contents that are sufficiently high to suggest euxinic conditions (Scott and Lyons, 2012). Although ORM deposited from strongly euxinic bottom waters are most likely to capture a seawater-like δ^{98}Mo signature, straightforward interpretation of the record is complicated by the likelihood that the δ^{98}Mo of ORM deposited from weakly euxinic waters will be offset significantly to values lower than those of seawater (as was observed for most Member IV samples). Hence, we use the highest δ^{98}Mo from each interval as the most conservative estimate of coeval seawater because the

546 highest δ^{98}Mo in an interval could still be fractionated from seawater (Dahl et al., 2010b;
547 Dickson et al., 2014).

548 An interval of low δ^{98}Mo and moderate Mo/TOC between 2050 Ma and 640 Ma points to
549 a generally moderate-sized oceanic Mo reservoir that reflects a combination of pervasive
550 oxidative weathering and redox-stratified oceans (oxic surface waters, euxinic waters at mid-
551 depths along productive ocean margins, and ferruginous deep waters; Arnold et al., 2004; Scott
552 et al., 2008; Kendall et al., 2009a, 2011; Dahl et al., 2010b, 2011; Planavsky et al., 2011; Poulton
553 and Canfield, 2011; Lyons et al., 2014). Elemental and isotopic mass balance models indicate
554 that the oceanic Mo reservoir probably stayed below 20% of modern levels because of
555 pronounced Mo burial in sulfidic marine environments (Scott et al., 2008; Dahl et al., 2011;
556 Reinhard et al., 2013). Our new Mo data from the Black River Dolomite suggests that a similar
557 redox character prevailed at ca. 640 Ma, consistent with moderate Mo/TOC in ca. 660 Ma
558 euxinic ORM from the lower part of the Datangpo Formation, South China (Li et al., 2012).

559 In contrast, Baldwin et al. (2013) infer a higher δ^{98}Mo of ~1.8 ‰ for middle Cryogenian
560 seawater based on analyses of jasper beds from the dropstone-bearing (syn-glacial) Rapitan iron
561 formation (NW Canada). This value was calculated assuming Mo isotope fractionation during
562 adsorption to hematite. An alternative to this local-scale interpretation is that high seawater
563 δ^{98}Mo was generated globally by preferential removal of isotopically light Mo from a small
564 oceanic Mo reservoir to abundant Fe oxyhydr(oxides). Under icehouse conditions where the
565 oceans are stagnant and predominantly anoxic (thus Mo-poor) beneath widespread ice cover
566 (with low sulfur inputs), Fe oxyhydr(oxides) would likely precipitate as a result of Fe^{2+} oxidation
567 via oxygenic photosynthesis beneath thin ice cover or via photoferrotrophy (Kirschvink, 1992;
568 Canfield and Raiswell, 1999; Hoffman and Schrag, 2002). As another (non-glacial) example

569 involving extensive ocean anoxia, preferential removal of isotopically light Mo from a small
570 oceanic Mo inventory to Fe oxyhydr(oxides) was suggested to account for high δ^{98}Mo in late
571 Archean euxinic ORM deposited before the Great Oxidation Event (Duan et al., 2010; Czaja et
572 al., 2012).

573 High Mo/TOC ratios from ORM of lower Member II near the base of the Doushantuo
574 Formation indicate extensive ocean oxygenation at ca. 632 Ma (Sahoo et al., 2012). Otherwise,
575 geochemical data from early and middle Ediacaran sedimentary successions are consistent with
576 less oxygenated conditions, except following the ca. 580 Ma Gaskiers glaciation and at ca. 560-
577 551 Ma (Canfield et al., 2007, 2008; McFadden et al., 2008; Li et al., 2010; Johnston et al., 2012;
578 Och and Shields-Zhou, 2012). Future work is required to determine if additional episodes of
579 extensive ocean oxygenation also took place during early and middle Neoproterozoic time.

580 Late Ediacaran ocean oxygenation is roughly coincident with key steps in the radiation of
581 animals. Weakly calcified tubular metazoans (e.g., *Cloudina*) and their predators appeared before
582 548.8 ± 1 Ma (Bengston and Zhao, 1992; Grotzinger et al., 1995; Warren et al., 2012).
583 Macroscopic motile bilaterians (e.g., *Kimberella*) and their trace fossils appear in the rock record
584 by 555.3 ± 0.3 Ma and 585 ± 3 Ma, respectively (Martin et al., 2000; Fedonkin et al., 2007; Liu
585 et al., 2010; Pecoits et al., 2012; Rogov et al., 2012). Regionally stable ocean oxygenation
586 following the Gaskiers glaciation is temporally associated with the appearance of soft-bodied
587 Ediacaran macroscopic fauna (Canfield et al., 2007; Narbonne et al., 2009; Xiao and Laflamme,
588 2009; Wilby et al., 2011; Johnston et al., 2012). However, surface ocean oxygen levels during
589 earlier Neoproterozoic time were not necessarily low enough to preclude the existence of small
590 bilaterians (Sperling et al., 2013a; Planavsky et al., 2014). Furthermore, ecological and genetic
591 factors were likely important driving forces for metazoan evolution (e.g., Butterfield, 2009;

592 Erwin et al., 2011; Penny et al., 2014). Disentangling the relative importance of environmental,
593 ecological, and genetic factors is difficult given the current resolution of geochemical and
594 paleontological datasets. However, it is likely that the initial episodes of extensive ocean
595 oxygenation helped accelerate the radiation of Ediacaran metazoans in tandem with ecological
596 triggers, because more complex food webs and larger metazoans would be supported by higher
597 oxygen levels (Sperling et al., 2013b). High δ^{98}Mo and high Mo/TOC from early Cambrian
598 ORM (Wille et al., 2008) and high δ^{98}Mo from phosphorites (Wen et al., 2011) suggest at least
599 transient occurrences of widespread ocean oxygenation around the time of the Cambrian
600 Explosion.

601 A return to generally less oxygenated deep oceans with expanded sulfidic marine
602 environments (possibly triggered by a significant increase in bioturbation; Boyle et al., 2014) is
603 marked by lower δ^{98}Mo and lower Mo/TOC at 520-440 Ma, except for one example of high
604 δ^{98}Mo in the late Ordovician (Dahl et al., 2010b; Zhou et al., 2012). This time interval includes
605 an episode of extreme O_2 deficiency during the ca. 500 Ma Steptoean Positive Carbon Isotope
606 Excursion (SPICE) (Gill et al., 2011). Because the δ^{98}Mo and Mo/TOC proxies are highly
607 sensitive to changes in the extent of water column euxinia over a small percentage of the
608 seafloor, it is difficult to infer the redox state of early Paleozoic deep oceans using Mo alone. A
609 return to Proterozoic-style ferruginous deep ocean conditions (Planavsky et al., 2011; Poulton
610 and Canfield, 2011) is not strictly required to explain the low δ^{98}Mo and moderate Mo/TOC at
611 520-440 Ma despite the similarities in Mo data with the ca. 2050-640 Ma interval. Compilations
612 of Cr and U concentrations in ORM suggest a first-order increase in the seawater inventory of
613 these metals in the early Paleozoic compared to the Precambrian (Reinhard et al., 2013; Partin et
614 al., 2013). The oceanic mass balances of Cr and U are less sensitive to water column euxinia

615 compared to Mo. Taking this into account, the Mo data at 520-440 Ma can be interpreted as
616 reflecting mid-depth euxinic waters along productive ocean margins and weakly oxygenated
617 deep waters (cf. Dahl et al., 2010b).

618 High δ^{98}Mo and generally high Mo/TOC in later Phanerozoic ORM indicates that
619 widespread and persistent ocean oxygenation was probably established by 390 Ma, possibly
620 coincident with the diversification of vascular land plants (Dahl et al., 2010b). Widespread ocean
621 oxygenation during younger Phanerozoic time may have been interrupted only by sporadic, brief
622 intervals of expanded oceanic anoxia during which the oceanic Mo inventory and seawater
623 δ^{98}Mo became temporarily smaller and lower, respectively (e.g., the Mesozoic examples in Fig.
624 4; Pearce et al., 2008, 2010; Westermann et al., 2014). The picture that emerges is an Ediacaran
625 to early Paleozoic interval of fluctuating ocean redox conditions that bridges the transition from
626 O_2-deficient Proterozoic oceans to widely oxygenated later Phanerozoic oceans.

627

628 ## 6. CONCLUSIONS

629

630 New U and Mo isotope data from Member IV ORM of the Doushantuo Formation point
631 to extensively oxygenated oceans during ca. 560-551 Ma, consistent with the previous
632 conclusion reached by Scott et al. (2008) on the basis of high Mo concentrations in Member IV.
633 The consistently high δ^{238}U values throughout Member IV, when corrected for isotope
634 fractionation accompanying U burial in ORM, point to high seawater δ^{238}U at 560-551 Ma and
635 hence a broadly similar oceanic redox character and oceanic U isotope mass balance as today.
636 Most of the Mo isotope data in Member IV are probably fractionated from seawater, consistent
637 with deposition from local bottom waters that were weakly sulfidic ($[H_2S]_{aq}$ <11 μM). High

Mo/U ratios also suggest the efficient transfer of isotopically light Mo to sediments by a local particulate Fe-Mn oxyhydroxide shuttle. However, an instance of high seawater δ^{98}Mo paired with high Mo/TOC occurs in the upper part of Member IV, again pointing to widespread ocean oxygenation. A temporal compilation of δ^{98}Mo and associated Mo/TOC reveals that ocean oxygenation was probably not a linear process. It is likely that the late Neoproterozoic rise in atmospheric O_2 led to an Ediacaran-to-early-Phanerozoic interval of dynamic ocean redox changes, which bridged the transition from predominantly O_2-deficient Proterozoic oceans to widely oxygenated later Phanerozoic oceans.

ACKNOWLEDGEMENTS

This study was financially supported by the National Science Foundation, the NASA Astrobiology Institute, and the Agouron Institute. Support was provided to TWL by NSF-EAR and the NASA Exobiology and Astrobiology programs. BK is supported by a NSERC Discovery Grant (RGPIN-435930). Constructive comments by three anonymous reviewers improved the manuscript.

APPENDIX A

A.1. Black River Dolomite samples

The Western Tasmania Terrane is suggested to have formed part of the East Antarctic margin of the Australia-East Antarctica continental block during the Neoproterozoic before

661 rifting away at ca. 580 Ma (Direen and Crawford, 2003; Meffre et al., 2004; Berry et al., 2008).
662 In northwestern Tasmania, the ca. 740-542 Ma Togari Group begins locally with the coarse-
663 grained Forest Conglomerate, which in turn is overlain by 600 m of stromatolitic dolostones,
664 organic-rich chert and mudrock, and diamictite of the Black River Dolomite (Calver, 1998;
665 Calver and Walter, 2000). These lithologies record continental shelf deposition, with the organic-
666 rich units representing sedimentation in deeper-water environments. Overlying the Black River
667 Dolomite are fine-grained mudrocks, volcaniclastic arenites, rhyodacite, diamictite, and tholeiitic
668 basalt of the 1 km thick Kannunah Subgroup, deposited in a rift setting (Calver et al., 2004). In
669 the Forest-1 core, the top of the Black River Dolomite is represented by 40 m of pyritic ORM
670 with subordinate carbonate (Calver and Walter, 2000). Samples of finely laminated pyritic ORM
671 were obtained from the lower part of this interval at ca. 828 m and 836 m depth in Forest-1. A
672 precise Re-Os depositional age of 640.7 ± 4.7 Ma (MSWD = 0.91) was obtained from the ORM
673 at 836 m (Kendall et al., 2009b). Molybdenum concentration and isotope data, sedimentary Fe
674 speciation analyses, and TOC data were obtained using the same methods described in section 3
675 (Analytical Methods). Data are presented in Table A.1.
676
677 **REFERENCES**
678
679 Algeo T. J. and Lyons T. W. (2006) Mo-total organic carbon covariation in modern anoxic
680 marine environments: Implications for analysis of paleoredox and paleohydrographic
681 conditions. *Paleoceanogr.* **21**, PA1016.
682 Algeo T. J. and Tribovillard N. (2009) Environmental analysis of paleoceanographic systems
683 based on molybdenum-uranium covariation. *Chem. Geol.* **268**, 211-225.

Andersen M. B., Romaniello S., Vance D., Little S. H., Herdman R. and Lyons T. W. (2014) A modern framework for the interpretation of $^{238}U/^{235}U$ in studies of ancient ocean redox. *Earth Planet. Sci. Lett.* **400**, 184-194.

Anderson R. F., Fleischer M. Q. and LeHuray A. P. (1989) Concentration, oxidation state, and particulate flux of uranium in the Black Sea. *Geochim. Cosmochim. Acta* **53**, 2215-2224.

Anderson T. F. and Raiswell R. (2004) Sources and mechanisms for the enrichment of highly reactive iron in euxinic Black Sea sediments. *Am. J. Sci.* **304**, 203-233.

Archer C. and Vance D. (2008) The isotopic signature of the global riverine molybdenum flux and anoxia in the ancient oceans. *Nature Geosci.* **1**, 597-600.

Arnold G. L., Anbar A. D., Barling J. and Lyons T. W. (2004) Molybdenum isotope evidence for widespread anoxia in Mid-Proterozoic oceans. *Science* **304**, 87-90.

Arnold G. L., Lyons T. W., Gordon G. W. and Anbar A. D. (2012) Extreme change in sulfide concentrations in the Black Sea during the Little Ice Age reconstructed using molybdenum isotopes. *Geology* **40**, 595-598.

Asael D., Tissot F. L. H., Reinhard C. T., Rouxel O., Dauphas N., Lyons T. W., Ponzevera E., Liorzou C. and Chéron S. (2013) Coupled molybdenum, iron and uranium stable isotopes as oceanic paleoredox proxies during the Paleoproterozoic Shunga Event. *Chem. Geol.* **362**, 193-210.

Azrieli-Tal I., Matthews A., Bar-Matthews M., Almogi-Labin A., Vance D., Archer C. and Teutsch N. (2014) Evidence from molybdenum and iron isotopes and molybdenum-uranium covariation for sulphidic bottom waters during Eastern Mediterranean sapropel S1 formation. *Earth Planet. Sci. Lett.* **393**, 231-242.

706 Bailey J. V., Joye S. B., Kalanetra K. M., Flood B. E. and Corsetti F. A. (2007) Evidence of giant
707 sulphur bacteria in Neoproterozoic phosphorites. *Nature 445*, 198-201.
708 Baldwin G. J., Nägler T. F., Greber N. D., Turner E. C. and Kamber B. S. (2013) Mo isotopic
709 composition of the mid-Neoproterozoic ocean: An iron formation perspective. *Precambr.*
710 *Res.* **230**, 168-178.
711 Barling J. and Anbar A. D. (2004) Molybdenum isotope fractionation during adsorption by
712 manganese oxides. *Earth Planet. Sci. Lett.* **217**, 315-329.
713 Barling J. Arnold G. L. and Anbar A. D. (2001) Natural mass-dependent variations in the
714 isotopic composition of molybdenum. *Earth Planet. Sci. Lett.* **193**, 447-457.
715 Barnes C. E. and Cochran J. K. (1990) Uranium removal in oceanic sediments and the oceanic U
716 balance. *Earth Planet. Sci. Lett.* **97**, 94-101.
717 Bengtson S. and Zhao Y. (1992) Predatorial borings in late Precambrian mineralized
718 exoskeletons. *Science* **257**, 367-369.
719 Berry R. F., Steele D. A., and Meffre S. (2008) Proterozoic metamorphism in Tasmania:
720 Implications for tectonic reconstructions. *Precambr. Res.* **166**, 387-396.
721 Boyle R. A., Dahl T. W., Dale A. W., Shields-Zhou G. A., Zhu M., Brasier M. D., Canfield D. E.
722 and Lenton T. M. (2014) Stabilization of the coupled oxygen and phosphorus cycles by
723 the evolution of bioturbation. *Nature Geosci.* **7**, 671-676.
724 Brennecka G. A., Herrmann A. D., Algeo T. J. and Anbar A. D. (2011a) Rapid expansion of
725 ocean anoxia immediately before the end-Permian mass extinction. *Proc. Natl. Acad. Sci.*
726 *USA* **108**, 17631-17634.

727 Brennecka G. A., Wasylenki L. E., Bargar J. R., Weyer S. and Anbar A. D. (2011b) Uranium
728 isotope fractionation during adsorption to Fe-Mn oxyhydroxides. *Environ. Sci. Tech.* **45**,
729 1370-1375.
730 Butterfield N. J. (2009) Oxygen, animals and oceanic ventilation: an alternative view. *Geobiol.*
731 **7**, 1-7.
732 Calver C. R. (1998) Isotope stratigraphy of the Neoproterozoic Togari Group, Tasmania. *Aust. J.*
733 *Earth Sci.* **45**, 865-874.
734 Calver C. R. (2000) Isotope stratigraphy of the Ediacaran (Neoproterozoic III) of the Adelaide
735 rift complex, Australia, and the overprint of water column stratification. *Precambr. Res.*
736 **100**, 121-150.
737 Calver C. R. and Walter M. R. (2000) The late Neoproterozoic Grassy Group of King Island,
738 Tasmania: correlation and palaeogeographic significance. *Precambr. Res.* **100**, 299-312.
739 Calver C. R., Black L. P., Everard J. L. and Seymour D. B. (2004) U-Pb zircon age constraints
740 on late Neoproterozoic glaciation in Tasmania. *Geology* **32**, 893-896.
741 Canfield D. E. and Raiswell R. (1999) The evolution of the sulfur cycle. *Amer. J. Sci.* **299**, 697-
742 723.
743 Canfield D. E., Poulton S. W. and Narbonne G. M. (2007) Late-Neoproterozoic deep-ocean
744 oxygenation and the rise of animal life. *Science* **315**, 92-95.
745 Canfield D. E., Poulton S. W., Knoll A. H., Narbonne G. M., Ross G., Goldberg T. and Strauss
746 H. (2008) Ferruginous conditions dominated later Neoproterozoic deep-water chemistry.
747 *Science* **321**, 949-952.

748 Chappaz A., Lyons T. W., Gregory D. D., Reinhard C. T., Gill B. C., Li C. and Large R. R.
749 (2014) Does pyrite act as an important host for molybdenum in modern and ancient
750 euxinic sediments? *Geochim. Cosmochim. Acta* **126**, 112-122.
751 Chen D. F., Dong W. Q., Zhu B. Q. and Chen X. P. (2004) Pb-Pb ages of Neoproterozoic
752 Doushantuo phosphorites in South China: constraints on early metazoan evolution and
753 glaciation events. *Precambr. Res.* **132**, 123-132.
754 Chen L., Xiao S., Pang K., Zhou C. and Yuan X. (2014) Cell differentiation and germ-soma
755 separation in Ediacaran animal embryo-like fossils. *Nature* **516**, 238-241.
756 Chen Z., Bengtson S., Zhou C., Hua H. and Yue Z. (2008) Tube structure and original
757 composition of *Sinotubulites*: Shelly fossils from the late Neoproterozoic in southern
758 Shaanxi, China. *Lethaia* **41**, 37-45.
759 Condon D., Zhu M., Bowring S., Wang W., Yang A. and Jin Y. (2005) U-Pb ages from the
760 Neoproterozoic Doushantuo Formation, China. *Science* **308**, 95-98.
761 Czaja A. D., Johnson C. M., Roden E. E., Beard B. L., Voegelin A. R., Nägler T. F., Beukes N.
762 J. and Wille M. (2012) Evidence for free oxygen in the Neoarchean ocean based on
763 coupled iron-molybdenum isotope fractionation. *Geochim. Cosmochim. Acta* **86**, 118-
764 137.
765 Dahl T. W., Anbar A. D., Gordon G. W., Rosing M. T., Frei R. and Canfield D. E. (2010a) The
766 behavior of molybdenum and its isotopes across the chemocline and in the sediments of
767 sulfidic Lake Cadagno, Switzerland. *Geochim. Cosmochim. Acta* **74**, 144-163.
768 Dahl T. W., Hammarlund E. U., Anbar A. D., Bond D. P. G., Gill B. C., Gordon G. W., Knoll A.
769 H., Nielsen A. T., Schovsbo N. H. and Canfield D. E. (2010b) Devonian rise in

atmospheric oxygen correlated to the radiations of terrestrial plants and large predatory fish: *Proc. Natl. Acad. Sci. USA* **107**, 17911-17915.

Dahl T. W., Canfield D. E., Rosing M. T., Frei R. E., Gordon G. W., Knoll A. H. and Anbar A. D. (2011) Molybdenum evidence for expansive sulfidic water masses in ~750 Ma oceans. *Earth Planet. Sci. Lett.* **311**, 264-274.

Dahl T. W., Chappaz A., Fitts J. P. and Lyons T. W. (2013) Molybdenum reduction in a sulfidic lake: Evidence from X-ray absorption fine-structure spectroscopy and implications for the Mo paleoproxy. *Geochim. Cosmochim. Acta* **103**, 213-231.

Dahl T. W., Boyle R. A., Canfield D. E., Connelly J. N., Gill B. C., Lenton T. M. and Bizzaro M. (2014) Uranium isotopes distinguish two geochemically distinct stages during the later Cambrian SPICE event. *Earth Planet. Sci. Lett.* **401**, 313-326.

Dickson A. J. and Cohen A. S. (2012) A molybdenum isotope record of Eocene Thermal Maximum 2: Implications for global ocean redox during the early Eocene. *Paleoceanogr.* **27**, PA3230.

Dickson A. J., Cohen A. S. and Coe A. L. (2012) Seawater oxygenation during the Paleocene-Eocene Thermal Maximum. *Geology* **40**, 639-642.

Dickson A. J., Cohen A. S. and Coe A. L. (2014) Continental margin molybdenum isotope signatures from the early Eocene. *Earth Planet. Sci. Lett.* **404**, 389-395.

Direen N. G. and Crawford A. J. (2003) Fossil seaward-dipping reflector sequences preserved in southeastern Australia: a 600 Ma volcanic passive margin in eastern Gondwanaland. *J. Geol. Soc. London* **160**, 985-990.

791 Duan Y., Anbar A. D., Arnold G. L., Lyons T. W., Gordon G. W. and Kendall B. (2010)
792 Molybdenum isotope evidence for mild environmental oxygenation before the Great
793 Oxidation Event. *Geochim. Cosmochim. Acta* **74**, 6655-6668.
794 Dunk R. M., Mills R. A. and Jenkins W. J. (2002) A reevaluation of the oceanic uranium budget
795 for the Holocene. *Chem. Geol.* **190**, 45-67.
796 Erickson B. E. and Helz G. R. (2000) Molybdenum (VI) speciation in sulfidic waters: Stability
797 and lability of thiomolybdates. *Geochim. Cosmochim. Acta* **64**, 1149-1158.
798 Erwin D. H., Laflamme M., Tweedt S. M., Sperling E. A., Pisani D. and Peterson K. J. (2011)
799 The Cambrian conundrum: Early divergence and later ecological success in the early
800 history of animals. *Science* **334**, 1091-1097.
801 Fan H., Zhu X., Wen H., Yan B., Li J., Feng L. (2014) Oxygenation of Ediacaran ocean recorded
802 by iron isotopes. *Geochim. Cosmochim. Acta* **140**, 80-94.
803 Fedonkin M. A., Simonetta A. and Ivantsov A. Y. (2007) New data on *Kimberella*, the Vendian
804 mollusc-like organism (White Sea region, Russia): paleoecological and evolutionary
805 implications. *Geol. Soc. Lon. Spec. Publ.* **286**, 157-179.
806 Fike D. A., Grotzinger J. P., Pratt L. M. and Summons R. E. (2006) Oxidation of the Ediacaran
807 ocean. *Nature* **444**, 744-747.
808 Frei R., Gaucher C., Stolper D. and Canfield D. E. (2013) Fluctuations in late Neoproterozoic
809 atmospheric oxidation – Cr isotope chemostratigraphy and iron speciation of the late
810 Ediacaran lower Arroyo del Soldado Group (Uruguay). *Gondwana Res.* **23**, 797-811.
811 Gill B. C., Lyons T. W., Young S. A., Kump L. R., Knoll A. H. and Saltzman M. R. (2011)
812 Geochemical evidence for widespread euxinia in the later Cambrian ocean. *Nature* **469**,
813 80-83.

814 Goldberg T., Archer C., Vance D., Thamdrup B., McAnena A. and Poulton S. W. (2012)
815 Controls on Mo isotope fractionations in a Mn-rich anoxic marine sediment, Gullmar
816 Fjord, Sweden. *Chem. Geol.* **296-297**, 73-82.
817 Goldberg T., Gordon G., Izon G., Archer C., Pearce C. R., McManus J., Anbar A. D. and
818 Rehkämper M. (2013) Resolution of inter-laboratory discrepancies in Mo isotope data: an
819 intercalibration. *J. Anal. At. Spectrom.* **28**, 724-735.
820 Gordon G. W., Lyons T. W., Arnold G. L., Roe J., Sageman B. B. and Anbar A. D. (2009) When
821 do black shales tell molybdenum isotope tales? *Geology* **37**, 535-538.
822 Goto K. T., Anbar A. D., Gordon G. W., Romaniello S. J., Shimoda G., Takaya Y., Tokumaru
823 A., Nozaki T., Suzuki K., Machida S., Hanyu T. and Usui A. (2014) Uranium isotope
824 systematics of ferromanganese crusts in the Pacific Ocean: Implications for the marine
825 $^{238}U/^{235}U$ isotope system. *Geochim. Cosmochim. Acta* **146**, 43-58.
826 Grotzinger J. P., Bowring S. A., Saylor B. Z. and Kaufman A. J. (1995) Biostratigraphic and
827 geochronologic constraints on early animal evolution. *Science* **270**, 598-604.
828 Grotzinger J. P., Fike D. A. and Fischer W. W. (2011) Enigmatic origin of the largest-known
829 carbon isotope excursion in Earth's history. *Nature Geosci.* **4**, 285-292.
830 Guan C., Zhou C., Wang W., Wan B., Yuan X. and Chen Z. (2014) Fluctuation of shelf basin
831 redox conditions in the early Ediacaran: Evidence from Lantian Formation black shales in
832 South China. *Precambr. Res.* **245**, 1-12.
833 Hannah J. L., Stein H. J., Wieser M. E., de Laeter J. R. and Varner M. D. (2007) Molybdenum
834 isotope variations in molybdenite: Vapor transport and Rayleigh fractionation of Mo.
835 *Geology* **35**, 703-706.

836 Helz G. R., Miller C. V., Charnock J. M., Mosselmans J. F. W, Pattrick R. A. D, Garner C. D.
837 and Vaughan D. J. (1996) Mechanism of molybdenum removal from the sea and its
838 concentration in black shales: EXAFS evidence. *Geochim. Cosmochim. Acta* **60**, 3631-
839 3642.
840 Helz G. R., Vorlicek T. P. and Kahn M. D. (2004) Molybdenum scavenging by iron
841 monosulfide. *Environ. Sci. Tech.* **38**, 4263-4268.
842 Helz G. R., Bura-Nakić E., Mikac N. and Ciglenečki I. (2011) New model for molybdenum
843 behavior in euxinic waters. *Chem. Geol.* **284**, 323-332.
844 Herrmann A. D., Kendall B., Algeo T. J., Gordon G. W., Wasylenki L. E. and Anbar A. D.
845 (2012) Anomalous molybdenum isotope trends in Upper Pennsylvanian euxinic facies:
846 Significance for use of δ^{98}Mo as a global marine redox proxy. *Chem. Geol.* **324-325**, 87-
847 98.
848 Hoffman P. F. and Schrag D. P. (2002) The snowball Earth hypothesis: testing the limits of
849 global change. *Terra Nova* **14**, 129-155.
850 Huldtgren T., Cunningham J. A., Yin C., Stampanoni M., Marone F., Donoghue P. C. J and
851 Bengtson S. (2011) Fossilized nuclei and germination structures identify Ediacaran
852 "animal embryos" as encysting protists. *Science* **334**, 1696-1699.
853 Jiang G., Sohl L. E. and Christie-Blick N. (2003) Neoproterozoic stratigraphic comparison of the
854 Lesser Himalaya (India) and Yangtze block (South China): Paleogeographic implications.
855 *Geology* **31**, 917-920.
856 Jiang G., Kaufman A. J., Christie-Blick N., Zhang S. and Wu H. (2007) Carbon isotope
857 variability across the Ediacaran Yangtze platform in South China: Implications for a large
858 surface-to-deep ocean δ^{13}C gradient. *Earth Planet. Sci. Lett.* **261**, 303-320.

859 Jiang G., Shi X., Zhang S., Wang Y. and Xiao S. (2011) Stratigraphy and paleogeography of the
860 Ediacaran Doushantuo Formation (ca. 635-551 Ma) in South China. *Gondwana Res.* **19**,
861 831-849.
862 Johnston D. T., Poulton S. W., Goldberg T., Sergeev V. N., Podkovyrov V., Vorob'eva N. G.,
863 Bekker A. and Knoll A. H. (2012) Late Ediacaran redox stability and metazoan
864 evolution. *Earth Planet. Sci. Lett.* **335-336**, 25-35.
865 Johnston D. T., Poulton S. W., Tosca N. J., O'Brien T., Halverson G. P., Schrag D. P. and
866 Macdonald F. A. (2013) Searching for an oxygenation event in the fossiliferous
867 Ediacaran of northwestern Canada. *Chem. Geol.* **362**, 273-286.
868 Kaufman A. J., Jiang G., Christie-Blick N., Banerjee D. M. and Rai V. (2006) Stable isotope
869 record of the terminal Neoproterozoic Krol platform in the Lesser Himalayas of northern
870 India. *Precambr. Res.* **147**, 156-185.
871 Kendall B., Creaser R. A., Gordon G. W. and Anbar A. D. (2009a) Re-Os and Mo isotope
872 systematics of black shales from the Middle Proterozoic Velkerri and Wollogorang
873 Formations, McArthur Basin, northern Australia. *Geochim. Cosmochim. Acta* **73**, 2534-
874 2558.
875 Kendall B., Creaser R. A., Calver C. R., Raub T. D. and Evans D. A. D. (2009b) Correlation of
876 Sturtian diamictite successions in southern Australia and northwestern Tasmania by Re-
877 Os black shale geochronology and the ambiguity of “Sturtian”-type diamictite-cap
878 carbonate pairs as chronostratigraphic marker horizons. *Precambr. Res.* **172**, 301-310.
879 Kendall B., Gordon G. W., Poulton S. W. and Anbar A. D. (2011) Molybdenum isotope
880 constraints on the extent of late Paleoproterozoic ocean euxinia. *Earth Planet. Sci. Lett.*
881 **307**, 450-460.

882 Kendall B., Brennecka G. A., Weyer S. and Anbar A. D. (2013) Uranium isotope fractionation
883 suggests oxidative uranium mobilization at 2.50 Ga. *Chem. Geol.* **362**, 105-114.
884 Kikumoto R., Tahata M., Nishizawa M., Sawaki Y., Maruyama S., Shu D., Han J., Komiya T.,
885 Takai K. and Ueno Y. (2014) Nitrogen isotope chemostratigraphy of the Ediacaran and
886 Early Cambrian platform sequence at Three Gorges, South China. *Gondwana Res.* **25**,
887 1057-1069.
888 Kirschvink J. L. (1992) Late Proterozoic low-latitude global glaciation: the snowball Earth. In
889 *The Proterozoic Biosphere* (eds. J. W. Schopf and C. Klein), pp. 51-52. Cambridge
890 University Press.
891 Knoll A. H. (2011) The multiple origins of complex multicellularity. *Ann. Rev. Earth Planet. Sci.*
892 **39**, 217-239.
893 Knoll A. H. and Carroll S. B. (1999) Early animal evolution: Emerging views from comparative
894 biology and geology. *Science* **284**, 2129-2137.
895 Ku T. L., Knauss K. and Mathieu G. G. (1977) Uranium in the open ocean: concentration and
896 isotopic composition. *Deep Sea Res.* **24**, 1005-1017.
897 Langmuir D. (1978) Uranium solution-mineral equilibria at low temperatures with applications
898 to sedimentary ore deposits. *Geochim. Cosmochim. Acta* **42**, 547-569.
899 Le Guerroué E. (2010) Duration and synchroneity of the largest negative carbon isotope
900 excursion on Earth: The Shuram/Wonoka anomaly. *Compt. Rend. Geosci.* **342**, 204-214.
901 Lehmann B., Nägler T. F., Holland H. D., Wille M., Mao J., Pan J., Ma D. and Dulski P. (2007)
902 Highly metalliferous carbonaceous shale and Early Cambrian seawater. *Geology* **35**, 403-
903 406.

904 Lenton T. M., Boyle R. A., Poulton S. W., Shields-Zhou G. A. and Butterfield N. J. (2014) Co-
905 evolution of eukaryotes and ocean oxygenation in the Neoproterozoic Era. *Nature Geosc.*
906 **7**, 257-265.
907 Li C., Love G. D., Lyons T. W., Fike D. A., Sessions A. L. and Chu X. (2010) A stratified redox
908 model for the Ediacaran ocean: *Science* **328**, 80-83.
909 Li C., Love G. D., Lyons T. W., Scott C. T., Feng L., Huang J., Chang H., Zhang Q. and Chu X.
910 (2012) Evidence for a redox stratified Cryogenian marine basin, Datangpo Formation,
911 South China. *Earth Planet. Sci. Lett.* **331-332**, 246-256.
912 Liu A. G., McIlroy D. and Brasier M. D. (2010) First evidence for locomotion in the Ediacara
913 biota from the 565 Ma Mistaken Point Formation, Newfoundland. *Geology* **38**, 123-126.
914 Lowenstein T. K., Kendall B. and Anbar A. D. (2014) Chapter 8.21 – The geologic history of
915 seawater. In *The Oceans and Marine Geochemistry, Treatise on Geochemistry 2nd*
916 *Edition*, vol. 8 (eds. H. D. Holland and K. K. Turekian), pp. 569-622. Elsevier.
917 Lyons T. W. and Severmann S. (2006) A critical look at iron paleoredox proxies: New insights
918 from modern euxinic marine basins. *Geochim. Cosmochim. Acta* **70**, 5698-5722.
919 Lyons T. W., Reinhard C. T. and Planavsky N. J. (2014) The rise of oxygen in Earth's early
920 ocean and atmosphere. *Nature* **506**, 307-315.
921 Martin M. W., Grazhdankin D. V., Bowring S. A., Evans D. A. D., Fedonkin M. A. and
922 Kirschvink J. L. (2000) Age of Neoproterozoic bilaterian body and trace fossils, White
923 Sea, Russia: Implications for metazoan evolution. *Science* **288**, 841-845.
924 McFadden K. A., Huang J., Chu X., Jiang G., Kaufman A. J., Zhou C., Yuan X. and Xiao S.
925 (2008) Pulsed oxidation and biological evolution in the Ediacaran Doushantuo
926 Formation. *Proc. Natl. Acad. Sci. USA* **105**, 3197-3202.

McLennan S. M. (2001) Relationships between the trace element composition of sedimentary rocks and upper continental crust. *Geochem. Geophys. Geosyst.* **2** (2000GC000109).

Meffre S., Direen N. G., Crawford A. J. and Kamenetsky V. (2004) Mafic volcanic rocks on King Island, Tasmania: evidence for 579 Ma break-up in east Gondwana. *Precambr. Res.* **135**, 177-191.

Miller C. A., Peucker-Ehrenbrink B., Walker B. D. and Marcantonio F. (2011) Re-assessing the surface cycling of molybdenum and rhenium. *Geochim. Cosmochim. Acta* **75**, 7146-7179.

Mills D. B., Ward L. M., Jones C., Sweeten B., Forth M., Treusch A. H. and Canfield D. E. (2014) Oxygen requirements of the earliest animals. *Proc. Natl. Acad. Sci. USA* **111**, 4168-4172.

Montoya-Pino C., Weyer S., Anbar A. D., Pross J., Oschmann W., van de Schootbrugge B. and Arz H. W. (2010) Global enhancement of ocean anoxia during Oceanic Anoxic Event 2: a quantitative approach using U isotopes. *Geology* **38**, 315-318.

Morford J. L. and Emerson S. (1999) The geochemistry of redox sensitive trace metals in sediments. *Geochim. Cosmochim. Acta* **63**, 1735-1750.

Nägler T. F., Neubert N., Böttcher M. E., Dellwig O. and Schnetger B. (2011) Molybdenum isotope fractionation in pelagic euxinia: Evidence from the modern Black and Baltic Seas. *Chem. Geol.* **289**, 1-11.

Nägler T. F., Anbar A. D., Archer C., Goldberg T., Gordon G. W., Greber N. D., Siebert C., Sohrin Y. and Vance D. (2014) Proposal for an international molybdenum isotope measurement standard and data representation. *Geostand. Geoanal. Res.* doi: 10.1111/j.1751-908X.2013.00275.x

949 Nakagawa Y., Takano S., Firdaus M. L., Norisuye K., Hirata T., Vance D. and Sohrin Y. (2012)
950 The molybdenum isotopic composition of the modern ocean. *Geochem. J.* **46**, 131-141.
951 Narbonne G. M. and Gehling J. G. (2003) Life after snowball: The oldest complex Ediacaran
952 fossils. *Geology* **31**, 27-30.
953 Narbonne G. M., Laflamme M., Greentree C. and Trusler P. (2009) Reconstructing a lost world:
954 Ediacaran rangeomorphs from Spaniard's Bay, Newfoundland. *J. Paleontol.* **83**, 503-523.
955 Neubert N., Nägler T. F. and Böttcher M. E. (2008) Sulfidity controls molybdenum isotope
956 fractionation into euxinic sediments: Evidence from the modern Black Sea. *Geology* **36**,
957 775-778.
958 Noordmann J., Weyer S., Sharma M., Georg R., Rausch S. and Bach W. (2010) Fractionation of
959 $^{238}U/^{235}U$ in rivers and hydrothermal systems: constraints for the oceanic U isotope cycle.
960 *AGU Fall Meeting*, Abstract V31B-2330.
961 Noordmann J., Weyer S., Sharma M., Georg R. B., Rausch S. and Bach W. (2011) Fractionation
962 of $^{238}U/^{235}U$ during weathering and hydrothermal alteration. *Mineral. Mag.* **75**, 1548.
963 Och L. M. and Shields-Zhou G. A. (2012) The Neoproterozoic oxygenation event:
964 Environmental perturbations and biogeochemical cycling. *Earth-Sci. Rev.* **110**, 26-57.
965 Partin C. A., Bekker A., Planavsky N. J., Scott C. T., Bill B. C., Li C., Podkovyrov V., Maslov
966 A., Konhauser K. O., Lalonde S. V., Love G. D., Poulton S. W. and Lyons T. W. (2013)
967 Large-scale fluctuations in Precambrian atmospheric and oceanic oxygen levels from the
968 record of U in shales. *Earth Planet. Sci. Lett.* **369-370**, 284-293.
969 Pearce C. R., Cohen A. S., Coe A. L. and Burton K. W. (2008) Molybdenum isotope evidence
970 for global ocean anoxia coupled with perturbations to the carbon cycle during the Early
971 Jurassic. *Geology* **36**, 231-234.

Pearce C. R., Coe A. L. and Cohen A. S. (2010) Seawater redox variations during the deposition of the Kimmeridge Clay Formation, United Kingdom (Upper Jurassic): Evidence from molybdenum isotopes and trace metal ratios. *Paleoceanogr.* **25**, PA4213.

Pecoits E., Konhauser K. O., Aubet N. R., Heaman L. M., Veroslavsky G., Stern R. A. and Gingras M. K. (2012) Bilaterian burrows and grazing behavior at >585 million years ago. *Science* **336**, 1693-1696.

Penny A. M., Wood R., Curtis A., Bowyer F., Tostevin R. and Hoffman K.-H. (2014) Ediacaran metazoan reefs from the Nama Group, Namibia. *Science* **344**, 1504-1506.

Planavsky N. J., Rouxel O. J., Bekker A., Lalonde S. V., Konhauser K. O., Reinhard C. T. and Lyons T. W. (2010) The evolution of the marine phosphate reservoir. *Nature* **467**, 1088-1090.

Planavsky N. J., McGoldrick P., Scott C. T., Li C., Reinhard C. T., Kelly A. E., Chu X., Bekker A., Love G. D. and Lyons T. W. (2011) Widespread iron-rich conditions in the mid-Proterozoic ocean. *Nature* **477**, 448-451.

Planavsky N. J., Reinhard C. T., Wang X., Thomson D., McGoldrick P., Rainbird R. H., Johnson T., Fischer W. W. and Lyons T. W. (2014) Low Mid-Proterozoic atmospheric oxygen levels and the delayed rise of animals. *Science* **346**, 635-638.

Poulson R. L., Siebert C., McManus J. and Berelson W. M. (2006) Authigenic molybdenum isotope signatures in marine sediments. *Geology* **34**, 617-620.

Poulson Brucker R. L., McManus J., Severmann S. and Berelson W. M. (2009) Molybdenum behavior during early diagenesis: Insights from Mo isotopes. *Geochem. Geophys. Geosyst.* **10**, Paper 2008GC002180.

994 Poulton S. W. and Canfield D. E. (2005) Development of a sequential extraction procedure for
995 iron: implications for iron partitioning in continentally derived particulates. *Chem. Geol.*
996 **214**, 209-221.
997 Poulton S. W. and Canfield D. E. (2011) Ferruginous conditions: A dominant feature of the
998 ocean through Earth's history. *Elements* **7**, 107-112.
999 Poulton S. W. and Raiswell R. (2002) The low-temperature geochemical cycle of iron: From
1000 continental fluxes to marine sediment deposition. *Am. J. Sci.* **302**, 774-805.
1001 Poulton S. W., Fralick P. W. and Canfield D. E. (2004) The transition to a sulphidic ocean ~1.84
1002 billion years ago. *Nature* **431**, 173-177.
1003 Proemse B. C., Grasby S. E., Wieser M. E., Mayer B. and Beauchamp B. (2013) Molybdenum
1004 isotopic evidence for oxic marine conditions during the latest Permian extinction.
1005 *Geology* **41**, 967-970.
1006 Raiswell R. and Canfield D. E. (1998) Sources of iron for pyrite formation in marine sediments.
1007 *Am. J. Sci.* **298**, 219-245.
1008 Reinhard C. T., Planavsky N. J., Robbins L. J., Partin C. A., Gill B. C., Lalonde S. V., Bekker
1009 A., Konhauser K. O. and Lyons T. W. (2013) Proterozoic ocean redox and
1010 biogeochemical stasis. *Proc. Natl. Acad. Sci. USA* **110**, 5357-5362.
1011 Retallack G. J., Marconato A., Osterhout J. T., Watts K. E. and Bindeman I. T. (2014) Revised
1012 Wonoka isotopic anomaly in South Australia and Late Ediacaran mass extinction. *J.*
1013 *Geol. Soc. Lond.* **171**, 709-722.
1014 Romaniello S. J., Herrmann A. D. and Anbar A. D. (2013) Uranium concentrations and $^{238}U/^{235}U$
1015 isotope ratios in modern carbonates from the Bahamas: Assessing a novel paleoredox
1016 proxy. *Chem. Geol.* **362**, 305-316.

1017 Rogov V., Marusin V., Bykova N., Goy Y., Nagovitsin K., Kochnev B., Karlova G. and
1018 Grazhdankin D. (2012) The oldest evidence of bioturbation on Earth. *Geology* **40**, 395-
1019 398.
1020 Runnegar B. (1991) Precambrian oxygen levels estimated from the biochemistry and physiology
1021 of early eukaryotes. *Palaeogeogr. Palaeoclimatol. Palaeoecol.* **97**, 97-111.
1022 Sahoo S. K., Planavsky N. J., Kendall B., Wang X., Shi X., Scott C., Anbar A. D., Lyons T. W.
1023 and Jiang G. (2012) Ocean oxygenation in the wake of the Marinoan glaciation. *Nature*
1024 **489**, 546-549.
1025 Sawaki Y., Ohno T., Tahata M., Komiya T., Hirata T., Maruyama S., Windley B. F., Han J., Shu
1026 D. and Li Y. (2010) The Ediacaran radiogenic Sr isotope excursion in the Doushantuo
1027 Formation in the Three Gorges area, South China. *Precambr. Res.* **176**, 46-64.
1028 Schauble E. A. (2006) Equilibrium uranium isotope fractionation by nuclear volume and mass-
1029 dependent processes. *Eos Trans. AGU* **87**, Fall Meeting Suppl., Abstract V21B-0570.
1030 Schiffbauer J. D., Xiao S., Sharma K. S. and Wang G. (2012) The origin of intracellular
1031 structures in Ediacaran metazoan embryos. *Geology* **40**, 223-226.
1032 Scholz F., McManus J. and Sommer S. (2013) The manganese and iron shuttle in a modern
1033 euxinic basin and implications for molybdenum cycling at euxinic ocean margins. *Chem.*
1034 *Geol.* **355**, 56-68.
1035 Scott C. and Lyons T. W. (2012) Contrasting molybdenum cycling and isotopic properties in
1036 euxinic versus non-euxinic sediments and sedimentary rocks: Refining the paleoproxies.
1037 *Chem. Geol.* **324-325**, 19-27.
1038 Scott C., Lyons T. W., Bekker A., Shen Y., Poulton S. W., Chu X. and Anbar A. D. (2008)
1039 Tracing the stepwise oxygenation of the Proterozoic ocean. *Nature* **452**, 456-459.

1040 Siebert C., Nägler T. F., von Blanckenburg F. and Kramers J. D. (2003) Molybdenum isotope
1041 records as a potential new proxy for paleoceanography. *Earth Planet. Sci. Lett.* **211**, 159-
1042 171.
1043 Siebert C., McManus J., Bice A., Poulson R. and Berelson W. M. (2006) Molybdenum isotope
1044 signatures in continental margin marine sediments. *Earth Planet. Sci. Lett.* **241**, 723-733.
1045 Sperling E. A., Frieder C. A., Raman A. V., Girguis P. R., Levin L. A. and Knoll A. H. (2013a)
1046 Oxygen, ecology, and the Cambrian radiation of animals. *Proc. Natl. Acad. Sci. USA* **110**,
1047 13446-13451.
1048 Sperling E. A., Halverson G. P., Knoll A. H., Macdonald F. A. and Johnston D. T. (2013b) A
1049 basin redox transect at the dawn of animal life. *Earth Planet. Sci. Lett.* **371-372**, 143-155.
1050 Stirling C. H., Andersen M. B., Potter E. K. and Halliday A. H. (2007) Low-temperature isotopic
1051 fractionation of uranium. *Earth Planet. Sci. Lett.* **264**, 208-225.
1052 Tahata M., Ueno Y., Ishikawa T., Sawaki Y., Murakami K., Han J., Shu D., Li Y., Guo J.,
1053 Yoshida N. and Komiya T. (2013) Carbon and oxygen isotope chemostratigraphies of the
1054 Yangtze platform, South China: Decoding temperature and environmental changes
1055 through the Ediacaran. *Gondwana Res.* **23**, 333-353.
1056 Towe K. M. (1970) Oxygen-collagen priority and the early metazoan fossil record. *Proc. Natl.*
1057 *Acad. Sci. USA* **65**, 781-788.
1058 Tribovillard N., Riboulleau A., Lyons T. and Baudin F. (2004) Enhanced trapping of
1059 molybdenum by sulfurized marine organic matter of marine origin in Mesozoic
1060 limestones and shales. *Chem. Geol.* **213**, 385-401.
1061 Tribovillard N., Algeo T. J., Lyons T. and Riboulleau A. (2006) Trace metals as paleoredox and
1062 paleoproductivity proxies: An update. *Chem. Geol.* **232**, 12-32.

1063 Verbruggen A. *et al.* (2008) Preparation and Certification of IRMM-3636, IRMM-3636a, and
1064 IRMM-3636b. Institute for Reference Materials and Measurements, 27 pp.
1065 Wang J. and Li Z.-X. (2003) History of Neoproterozoic rift basins in South China: implications
1066 for Rodinia breakup. *Precambr. Res.* **261**, 303-320.
1067 Warren L. V., Pacheco M. L. A. F., Fairchild T. R., Simões M. G., Riccomini C., Boggiani P. C.
1068 and Cáceres A. A. (2012) The dawn of animal skeletogenesis: Ultrastructural analysis of
1069 the Ediacaran metazoan *Corumbella werneri*. *Geology* **40**, 691-694.
1070 Wasylenki L. E., Rolfe B. A., Weeks C. L., Spiro T. G. and Anbar A. D. (2008) Experimental
1071 investigation of the effects of temperature and ionic strength on Mo isotope fractionation
1072 during adsorption to manganese oxides. *Geochim. Cosmochim. Acta* **72**, 5997-6005.
1073 Weber B., Steiner M. and Zhu M. Y. (2007) Precambrian-Cambrian trace fossils from the
1074 Yangtze Platform (South China) and the early evolution of bilaterian lifestyles.
1075 *Palaeogeogr. Palaeoclimatol. Palaeoecol.* **254**, 328-349.
1076 Wen H., Carignan J., Zhang Y., Fan H., Cloquet C. and Liu S. (2011) Molybdenum isotopic
1077 records across the Precambrian-Cambrian boundary. *Geology* **39**, 775-778.
1078 Westermann S., Vance D., Cameron V., Archer C. and Robinson S. A. (2014) Heterogeneous
1079 oxygenation states in the Atlantic and Tethys oceans during Oceanic Anoxic Event 2.
1080 *Earth Planet. Sci. Lett.* **404**, 178-189.
1081 Weyer S., Anbar A. D., Gerdes A., Gordon G. W., Algeo T. J. and Boyle E. A. (2008) Natural
1082 fractionation of $^{238}U/^{235}U$. *Geochim. Cosmochim. Acta* **72**, 345-359.
1083 Wilby P. R., Carney J. N. and Howe M. P. A. (2011) A rich Ediacaran assemblage from eastern
1084 Avalonia: Evidence of early widespread diversity in the deep ocean. *Geology* **39**, 655-
1085 658.

1086 Wille M., Nägler T. F., Lehmann B., Schröder S. and Kramers J. D. (2008) Hydrogen sulphide
1087 release to surface waters at the Precambrian/Cambrian boundary. *Nature* **453**, 767-769.
1088 Xiao S. and Laflamme M. (2009) On the eve of animal radiation: Phylogeny, ecology and
1089 evolution of the Ediacaran biota. *Trends Ecol. Evol.* **24**, 31-40.
1090 Xiao S., Yuan X., Steiner M. and Knoll A. H. (2002) Macroscopic carbonaceous compressions
1091 in a terminal Proterozoic shale: A systematic reassessment of the Miaohe Biota, South
1092 China. *J. Paleontol.* **76**, 347-376.
1093 Xiao S., Shen B., Zhou C., Xie G. and Yuan X. (2005) A uniquely preserved Ediacaran fossil
1094 with direct evidence for a quilted bodyplan. *Proc. Natl. Acad. Sci. USA* **102**, 10227-
1095 10232.
1096 Xiao S., Zhou C. and Yuan X. (2007) Undressing and redressing Ediacaran embryos. *Nature*
1097 **446**, E9-E11.
1098 Xiao S., Knoll A. H., Schiffbauer J. D., Zhou C. and Yuan X. (2012) Comment on "Fossilized
1099 nuclei and germination structures identify Ediacaran animal embryos as encysting
1100 protists". *Science* 335, 1169.
1101 Xiao S., Zhou C., Liu P., Wang D. and Yuan X. (2014) Phosphatized acanthomorphic acritarchs
1102 and related microfossils from the Ediacaran Doushantuo Formation at Weng'an (South
1103 China) and their implications for biostratigraphic correlation. *J. Paleontol.* **88**, 1-67.
1104 Yin L., Zhu M., Knoll A. H., Yuan X., Zhang J. and Hu J. (2007) Doushantuo embryos
1105 preserved inside diapause egg cysts. *Nature* 446, 661-663.
1106 Yuan X., Chen Z., Xiao S., Zhou C. and Hua H. (2011) An early Ediacaran assemblage of
1107 macroscopic and morphologically differentiated eukaryotes. *Nature* **470**, 390-393.

Zhou C. and Xiao S. (2007) Ediacaran $\delta^{13}C$ chemostratigraphy of South China. *Chemical Geology* **237**, 89-108.

Zhou C., Xie G., McFadden K., Xiao S. and Yuan X. (2007) The diversification and extinction of Doushantuo-Pertatataka acritarchs in South China: causes and biostratigraphic significance. *Geol. J.* **42**, 229-262.

Zhou L., Wignall P. B., Su J., Feng Q., Xie S., Zhao L. and Huang J. (2012) U/Mo ratios and $\delta^{98/95}Mo$ as local and global redox proxies during mass extinction events. *Chem. Geol.* **324-325**, 99-107.

Zhu B., Becker H., Jiang S. -Y., Pi D. -H., Fischer-Gödde M. and Yang, J. -H. (2013) Re-Os geochronology of black shales from the Neoproterozoic Doushantuo Formation, Yangtze platform, South China. *Precambr. Res.* **225**, 67-76.

Zhu M., Zhang J. and Yang A. (2007) Integrated Ediacaran (Sinian) chronostratigraphy of South China. *Palaeogeogr. Palaeoclimatol. Palaeoecol.* **254**, 7-61.

FIGURE CAPTIONS

Fig. 1. (a) Paleogeographic map of the Yangtze platform at ~600 Ma showing the location of the Three Gorges region. (b) Geological map of the Yangtze Gorges area, showing the location of the Jiulongwan outcrop section. The enclosed region is expanded in (c) to show the location of the drill core section (Site 1), which is ~5 km away from the Jiulongwan section in the Three Gorges region. (d) Cross-section along line A-B in (c) showing the Neoproterozoic stratigraphy and location of the Site #1 core. Modified from Sawaki et al. (2010) and Tahata et al. (2013).

Fig. 2. Geochemical profiles through Member IV, Doushantuo Formation. Stratigraphic columns of the Jiulongwan outcrop section and the Site 1 drill core section are modified from McFadden et al. (2008) and Sawaki et al. (2010), respectively (NF = glaciogenic Nantuo Formation; DF = Dengying Formation). The ovals within the black shale in the Jiulongwan section represent dolomite nodules. The error bars in the isotope profiles denote the long-term reproducibility of our secondary standards (~0.15‰ for Mo and ~0.07 ‰ for U; 2SD). For clarity, individual sample error bars are not shown. Total organic carbon, total Fe, highly reactive Fe and pyrite Fe are denoted by TOC, Fe_T, Fe_{HR}, and Fe_{PY}, respectively. Sediments deposited from anoxic bottom waters typically have Fe_{HR}/Fe_T >0.38, and Fe_{PY}/Fe_{HR} distinguishes between euxinic (>0.7) and ferruginous (<0.7) conditions.

Fig. 3. (a) Mo EF versus U EF for the Member IV ORM. The dashed lines are equivalent to the molar Mo/U ratio for modern seawater (1× SW) and for a fraction of modern seawater (0.3× SW), following Algeo and Tribovillard (2009). Green squares = Jiulongwan outcrop section. Red triangles = Site 1 drill core section. Large filled symbols = samples with highest δ^{98}Mo from each section. (b) δ^{98}Mo versus δ^{238}U for the Member IV ORM, showing no correlation between the two isotope systems ($R^2 < 0.3$ for both sections). Symbols are the same as in (a).

Fig. 4. Temporal record of δ^{98}Mo and associated Mo/TOC data from euxinic ORM, since the end of the Great Oxidation Event. Large squares represent the highest δ^{98}Mo for that time, with other data represented by small circles (red: 2050-640 Ma; orange: 555-530 Ma; blue: 520-440 Ma; green: 390-0 Ma). (a) Mo isotope record over the past 2050 Ma, with the 800-0 Ma interval expanded in (b) (Dsh IV = Doushantuo Formation, Member IV). (c) Cross plot of average

Mo/TOC ratio versus highest δ^{98}Mo (Mo/TOC data is not available for all intervals). Black Sea euxinic sediments have low Mo/TOC because of basin restriction (Algeo and Lyons, 2006). Three Mesozoic intervals also have low Mo/TOC because of a transient expansion of ocean anoxia (the highest δ^{98}Mo from the Jurassic sections mark a return to widespread ocean oxygenation; Pearce et al., 2008, 2010; Westermann et al., 2014). (d) Temporal comparison of known episodes of extensive ocean oxygenation (green bars), the Shuram-Wonoka carbon isotope anomaly, and the appearance of complex macroscopic metazoans (modified from Sawaki et al., 2010). The extent of ocean oxygenation at the start of the Shuram excursion is not known (see text for discussion). Data sources: δ^{98}Mo (Barling et al., 2001; Arnold et al., 2004; Lehmann et al., 2007; Wille et al., 2008; Neubert et al., 2008; Pearce et al., 2008; 2010; Gordon et al., 2009; Kendall et al., 2009a, 2011; Dahl et al., 2010b, 2011; Dickson and Cohen, 2012; Dickson et al., 2012; Herrmann et al., 2012; Zhou et al., 2012; Asael et al., 2013; Proemse et al., 2013; Westermann et al., 2014; this study), Shuram-Wonoka anomaly (McFadden et al., 2008; Sawaki et al., 2010; Tahata et al., 2013), acanthomorph acritarchs (Yin et al., 2007; McFadden et al., 2008), animal embryos (Yin et al., 2007), Ediacara fossils (Narbonne and Gehling, 2003), motile metazoans (Liu et al., 2010; Pecoits et al., 2012), macroscopic motile bilaterians (Martin et al., 2000), and weakly calcified metazoans (Grotzinger et al., 1995).

1177 **Figure 1**

1178

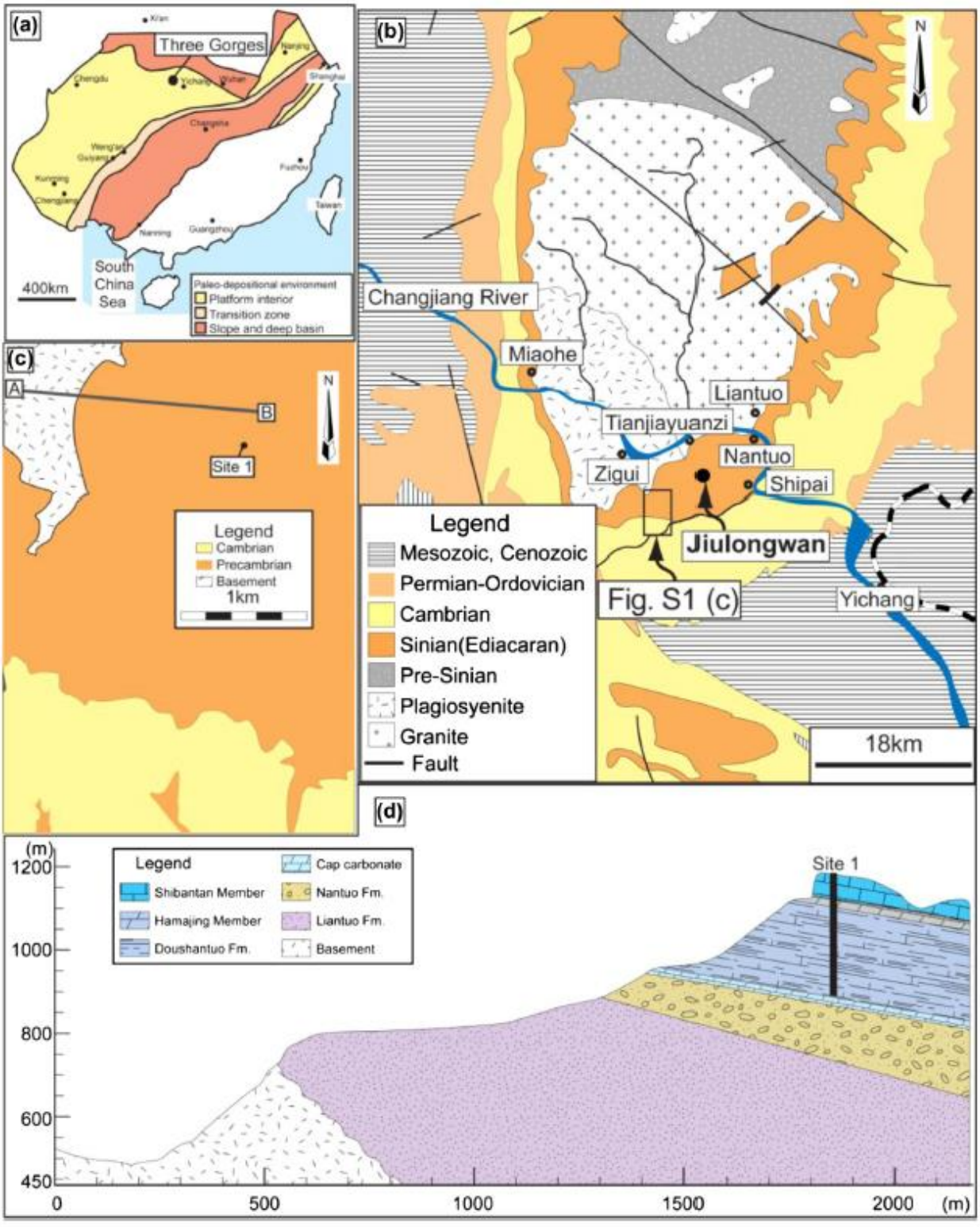

1179

Figure 2

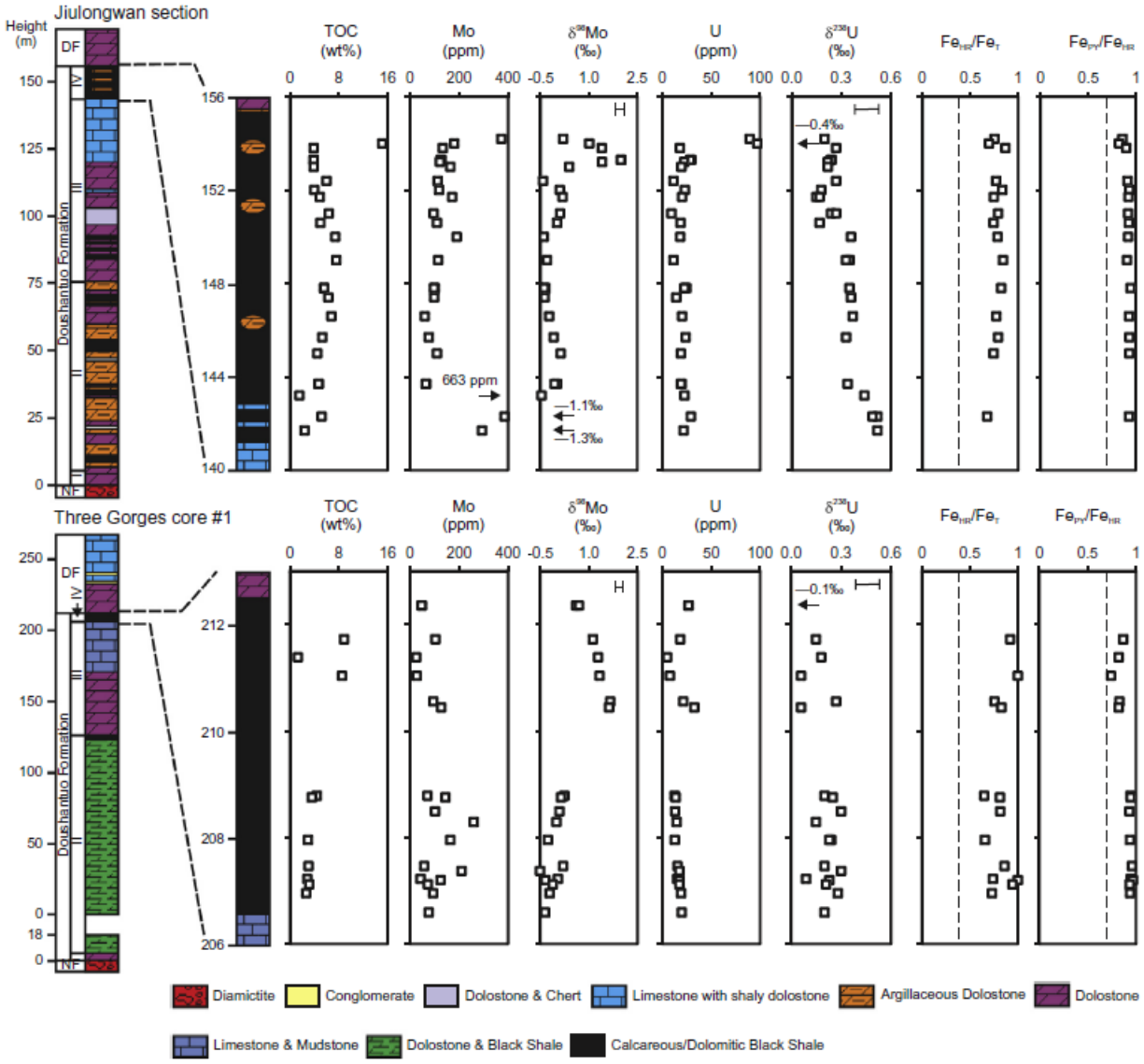
Jiulongwan section
Height (m)
DF
IV
III
II
I
NF
Doushantuo Formation
TOC (wt%)
Mo (ppm)
δ98Mo (‰)
U (ppm)
δ238U (‰)
FeHR/FeT
FePY/FeHR
663 ppm
1.1‰
1.3‰
0.4‰
Three Gorges core #1
0.1‰
Diamictite
Conglomerate
Dolostone & Chert
Limestone with shaly dolostone
Argillaceous Dolostone
Dolostone
Limestone & Mudstone
Dolostone & Black Shale
Calcareous/Dolomitic Black Shale

Figure 3

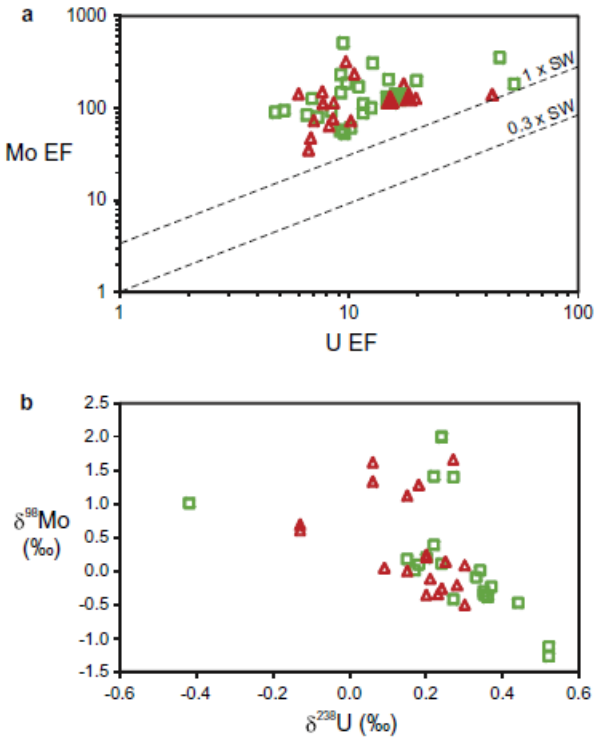
a
1000
100
10
1
Mo EF
1
10
100
U EF
1 x SW
0.3 x SW
b
2.5
2.0
1.5
1.0
0.5
0.0
-0.5
-1.0
-1.5
δ98Mo (‰)
-0.6
-0.4
-0.2
0.0
0.2
0.4
0.6
δ238U (‰)

Figure 4

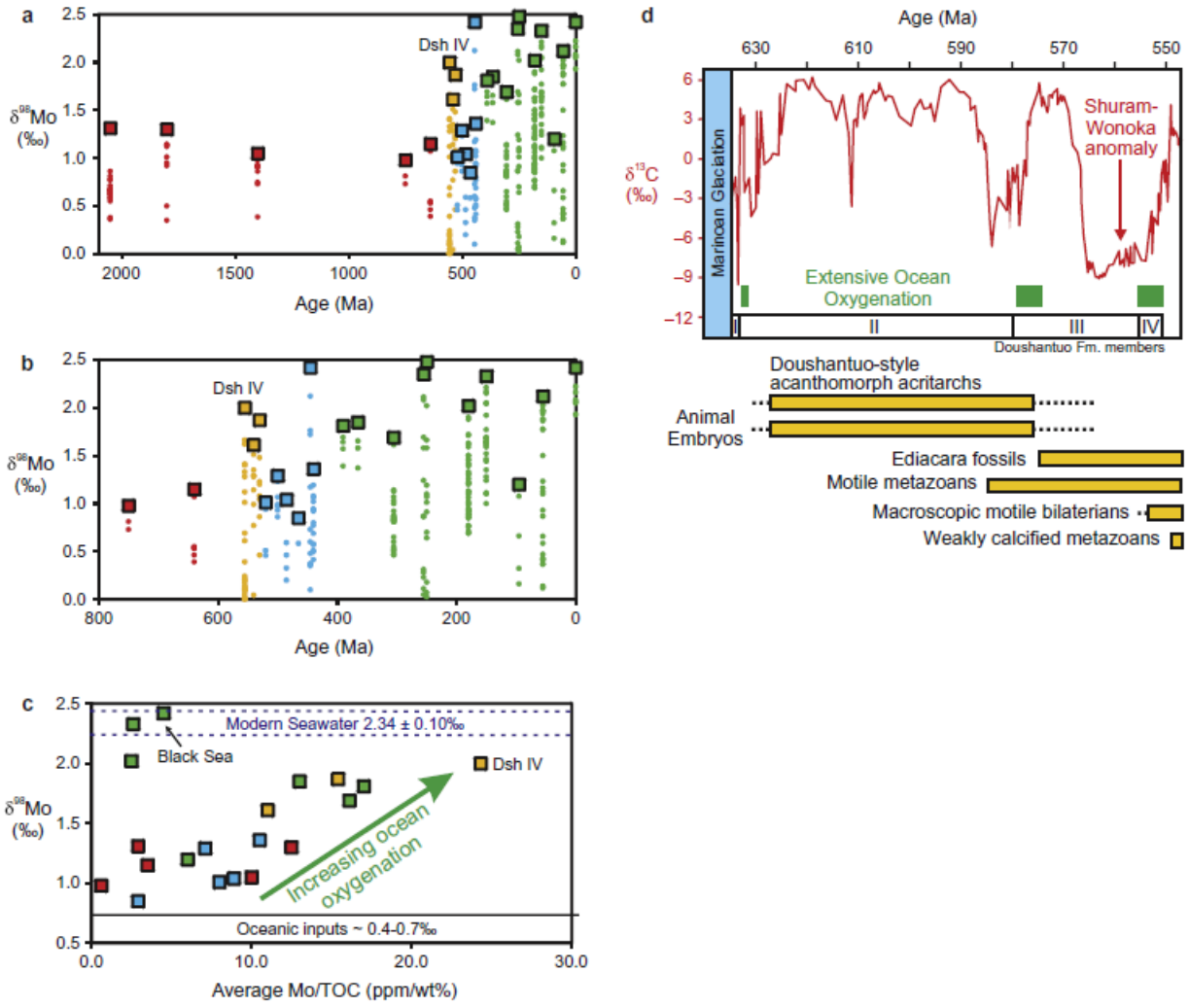
a
Dsh IV
δ98Mo (‰)
Age (Ma)
b
Dsh IV
δ98Mo (‰)
Age (Ma)
c
Modern Seawater 2.34 ± 0.10‰
Black Sea
Dsh IV
Increasing ocean oxygenation
Oceanic inputs ~ 0.4-0.7‰
δ98Mo (‰)
Average Mo/TOC (ppm/wt%)
d
Age (Ma)
Marinoan Glaciation
Shuram-Wonoka anomaly
Extensive Ocean Oxygenation
δ13C (‰)
I
II
III
IV
Doushantuo Fm. members
Doushantuo-style acanthomorph acritarchs
Animal Embryos
Ediacara fossils
Motile metazoans
Macroscopic motile bilaterians
Weakly calcified metazoans

Table 1

Table 1
Geochemical data for Member IV, Doushantuo Formation, Three Gorges region, South China.

Sample[a]	Height (m)	TOC[b] (wt%)	Al (wt%)	Mo (ppm)	Mo EF	Mo/TOC (ppm/wt%)	$\delta^{98}Mo$[c] (‰)	$\delta^{98}Mo$[d] (‰)	2SD Measured	2SD[e] Reported	n[f]	U (ppm)	U EF	$\delta^{238}U$ (‰)	2SD Measured	2SD[g] Reported	n[f]	Fe_{Carb} (wt%)	Fe_{Ox} (wt%)	Fe_{Mag} (wt%)	Fe_{PY} (wt%)	Fe_{HR}[h] (wt%)	Fe_T[i] (wt%)	Fe_{HR}/Fe_T	Fe_{PY}/Fe_{HR}
Jiulongwan Outcrop Section																									
HND 41.4	154.2		5.6	372	353		0.28	0.20	0.01	0.15	3	89	45	0.20	0.10	0.10	3	0.2	0.2	0.0	2.4	2.8	3.7	0.75	0.86
HN-23***	154.0	15.1	5.3	181	183	12	1.09	1.01	0.08	0.15	3	97	52	−0.42	0.09	0.09	3	0.2	0.1	0.0	1.9	2.3	3.3	0.70	0.83
HN-23rpt**	154.0													−0.37	0.07	0.07	3								
HND 41.0*	153.8	3.9	3.5	134	204	34	1.48	1.40	0.10	0.15	5	18	15	0.27	0.02	0.07	3	0.1	0.1	0.0	1.7	1.9	2.1	0.87	0.90
HND 40.5***	153.3	3.9	5.2	128	132	33	2.08	2.00	0.20	0.20	3	30	16	0.24	0.03	0.07	3						3.1		
HND 40.5rpt***	153.3	3.9	5.5	125	123	32	2.07	1.99	0.06	0.15	3	29	15	0.24	0.06	0.07	3						3.5		
HND 40.4	153.2		3.3	123	199		1.49	1.41	0.13	0.15	3	23	20	0.22	0.07	0.07	4						2.2		
HND 40.2*	153.0	3.9	5.2	165	171	42	0.47	0.39	0.07	0.15	5	20	11	0.22	0.04	0.07	3						2.6		
HND 39.6*	152.4	6.0	6.4	113	94	19	−0.34	−0.42	0.13	0.15	7	12	5.2	0.27	0.03	0.07	4	0.1	0.1	0.0	2.0	2.2	2.8	0.77	0.91
HND 39.2***	152.0	4.0	5.8	119	110	30	0.18	0.10	0.18	0.18	8	23	12	0.18	0.05	0.07	3	0.1	0.1	0.0	2.1	2.2	2.6	0.84	0.93
HND 38.9*	151.7	4.9	6.3	172	146	35	0.26	0.18	0.15	0.15	6	20	9.2	0.15	0.08	0.08	7	0.1	0.1	0.0	2.0	2.1	2.8	0.75	0.92
HND 38.9rpt*	151.7													0.17	0.01	0.07	4								
HND 38.2***	151.0	6.4	5.7	96	90	15	0.19	0.11	0.14	0.15	7	10	4.8	0.24	0.04	0.07	3	0.1	0.1	0.0	2.1	2.3	2.9	0.79	0.92
HND 38.2rpt***	151.0													0.27	0.06	0.07	3								
HND 37.8*	150.6	5.0	6.4	110	92	22	0.09	0.01	0.16	0.16	7	19	8.3	0.17	0.08	0.08	3	0.1	0.1	0.0	1.9	2.0	2.7	0.74	0.93
HND 36.85***	150.0	7.5	5.5	191	186	26	−0.31	−0.39	0.13	0.15	7	19	10	0.36	0.09	0.09	3	0.1	0.1	0.0	1.8	1.9	2.4	0.79	0.92
HND 36.2*	149.0	7.6	4.9	115	126	15	−0.22	−0.30	0.15	0.15	7	12	6.9	0.35	0.01	0.07	3	0.1	0.1	0.0	1.6	1.8	2.1	0.84	0.91
HND 36.2rpt*	149.0													0.33	0.05	0.07	3								
HND 35.0***	147.8	5.6	6.2	102	88	18	−0.27	−0.35	0.13	0.15	8	25	11	0.35	0.04	0.07	4	0.1	0.1	0.0	2.3	2.4	2.9	0.82	0.95
HND 35.0rpt***	147.8	5.6	5.2	98	100	17	−0.30	−0.38	0.07	0.15	3	23	12										2.8		
HND 34.6*	147.4	6.3	6.4	99	83	16	−0.29	−0.37	0.12	0.15	5	14	6.5	0.36	0.06	0.07	3						2.8		
HND 33.8*	146.6	6.8	6.1	60	53	8.8	−0.15	−0.23	0.12	0.15	5	20	10	0.37	0.09	0.09	3	0.1	0.1	0.0	1.8	1.9	2.5	0.77	0.93
HND 32.9***	145.7	5.3	6.8	77	61	14	−0.01	−0.09	0.19	0.19	8	24	10	0.33	0.08	0.08	3	0.1	0.1	0.0	2.1	2.2	2.8	0.79	0.93
HND 32.2*	145.0	4.5	7.5	110	79	24	0.21	0.13	0.17	0.17	7	19	7.3					0.1	0.1	0.0	2.3	2.5	3.3	0.75	0.93
HND 30.9***	143.7	4.7	6.3	66	57	14	0.09	0.01	0.19	0.19	6	20	9.1	0.34	0.06	0.07	3						3.1		
HND 30.9rpt***	143.7	4.7	6.0	64	57	14	0.02	−0.06	0.10	0.15	3	19	9.2										3.0		
HND 30.35***	143.2	1.6	6.9	663	512	420	−0.39	−0.47	0.15	0.15	7	23	9.4	0.44	0.08	0.08	7						2.5		
HND 29.5*	142.3	5.2	6.7	385	309	74	−1.04	−1.12	0.13	0.15	7	29	13	0.52	0.10	0.10	3	0.1	0.1	0.0	1.8	2.0	2.9	0.68	0.93
HND 29.5rpt*	142.3													0.49	0.11	0.11	6								
HND 28.85*	141.7	2.4	6.8	294	230	123	−1.19	−1.27	0.17	0.17	7	22	9.2	0.52	0.05	0.07	4						2.4		

(continued on next page)

Table 1 (*continued*)

Sample[a]	Height (m)	TOC[b] (wt%)	Al (wt%)	Mo (ppm)	Mo EF	Mo/TOC (ppm/wt%)	$\delta^{98}Mo$[c] (‰)	$\delta^{98}Mo$[d] (‰)	2SD Measured	2SD[e] Reported	n[f]	U (ppm)	U EF	$\delta^{238}U$ (‰)	2SD Measured	2SD[g] Reported	n[f]	Fe_{Carb} (wt%)	Fe_{Ox} (wt%)	Fe_{Mag} (wt%)	Fe_{PY} (wt%)	Fe_{HR}[h] (wt%)	Fe_T[i] (wt%)	Fe_{HR}/Fe_T	Fe_{PY}/Fe_{HR}
Three Gorges Core #1																									
40, 4 of 12	212.35		1.8	48	140		0.69	0.61	0.08	0.15	3	27	42	−0.13	0.07	0.07	4						1.1		
40, 4 of 12-rpt	212.35		1.9	48	139		0.77	0.69	0.06	0.15	3	27	42	−0.13	0.09	0.09	3						1.1		
S104012	211.72	8.9	3.1	104	181	12	1.20	1.12	0.07	0.15	4	19	17	0.15	0.05	0.07	3	0.1	0.1	0.0	1.3	1.5	1.7	0.92	0.87
S104103	211.38	1.3		25		19	1.36	1.28	0.21	0.21	7	5		0.18	0.10	0.10	4	0.1	0.1	0.0	0.6	0.8			0.82
S104106	211.03	8.6	1.2	27	126	3.2	1.41	1.33	0.14	0.15	5	8	20	0.06	0.01	0.07	4	0.1	0.1	0.0	0.4	0.6	0.6	1.00	0.74
41, 11 of 14	210.55		4.1	95	123		1.74	1.66	0.20	0.20	3	22	15	0.27	0.07	0.07	4	0.3	0.1	0.0	1.8	2.1	2.8	0.76	0.83
41, 13 of 14	210.44		5.2	127	132		1.70	1.62	0.17	0.17	3	33	18	0.06	0.05	0.07	3	0.4	0.1	0.0	2.3	2.9	3.4	0.83	0.82
S104206-A1	208.78	4.4	5.2	71	73	16	0.32	0.24	0.21	0.21	5	13	7.0	0.20	0.03	0.07	3	0.0	0.1	0.0	1.8	1.9	2.9	0.65	0.94
S104206-A2	208.75	3.6	5.2	145	150	40	0.22	0.14	0.13	0.15	4	14	7.6	0.25	0.03	0.07	3	0.1	0.1	0.0	2.2	2.4	2.9	0.81	0.94
42, 6 of 7, 1	208.49		4.9	102	111		0.17	0.09	0.09	0.15	3	13	7.7	0.30	0.10	0.10	5	0.1	0.1	0.0	1.8	2.0	2.4	0.82	0.93
42, 6 of 7, 6	208.29		4.4	261	320		0.08	0.00	0.18	0.18	3	15	10	0.15	0.14	0.14	7						2.3		
S104301B	207.95	3.0	6.2	164	142	55	−0.18	−0.26	0.16	0.16	5	13	6.0	0.24	0.07	0.07	4	0.0	0.1	0.0	1.8	1.9	2.9	0.66	0.94
S104301Brpt	207.95													0.23	0.08	0.08	4								
S104304	207.46	3.1	6.6	58	47	19	0.29	0.21	0.18	0.18	5	16	6.8	0.20	0.04	0.07	3	0.0	0.1	0.0	2.6	2.7	3.1	0.86	0.96
43, 4 of 6, A-1	207.37		4.8	210	234		−0.42	−0.50	0.11	0.15	3	18	11	0.30	0.06	0.07	4						2.5		
S104306	207.22	2.9	6.7	44	35	15	0.13	0.05	0.09	0.15	4	15	6.7	0.09	0.04	0.07	4	0.0	0.1	0.0	2.1	2.2	3.0	0.74	0.94
43, 6 of 6	207.20		5.9	125	114		−0.26	−0.34	0.11	0.15	3	18	8.6	0.23	0.05	0.07	4	0.0	0.1	0.0	3.2	3.3	2.9	1.00	0.97
S104401	207.12	3.2	6.1	73	64	23	−0.03	−0.11	0.17	0.17	5	17	8.2	0.21	0.05	0.07	4	0.1	0.1	0.0	2.5	2.7	2.8	0.94	0.93
S104402	206.95	2.7	6.6	94	76	35	−0.13	−0.21	0.13	0.15	4	19	8.5	0.28	0.10	0.10	3	0.1	0.1	0.0	2.0	2.2	3.0	0.73	0.94
44, 3 of 3	206.59		5.7	77	72		−0.27	−0.35	0.02	0.15	3	20	10	0.20	0.03	0.07	3						3.0		

[a] *Mo abundance, TOC, and DOP data from Scott et al. (2008); **Mo, Al, TOC, and Fe speciation data from Li et al. (2010); ***TOC data from McFadden et al. (2008).
[b] TOC = total organic carbon.
[c] Mo isotope data reported relative to RochMo2.
[d] Mo isotope data reported relative to NIST SRM 3134 = 0.25‰.
[e] Uncertainty is the 2SD of replicate measurements or 0.15‰, whichever is greater.
[f] Number of replicate analyses of the same sample solution.
[g] Uncertainty is the 2SD of replicate measurements or 0.07‰, whichever is greater.
[h] Fe_{HR} = Highly reactive Fe abundance = $Fe_{Carbonate}$ (Fe_{Carb}) + $Fe_{Ferric\text{-}Oxide}$ (Fe_{Ox}) + $Fe_{Magnetite}$ (Fe_{Mag}) + Fe_{Pyrite} (Fe_{PY}).
[i] Fe_T = Total Fe abundance.

Table A.1

Table A.1
Geochemical data for the Black River Dolomite, Tasmania.

Sample	Depth (m)	TOC[a] (wt%)	Al (wt%)	Mo (ppm)	Mo EF	Mo/TOC (ppm/wt%)	$\delta^{98}Mo$[b] (‰)	$\delta^{98}Mo$[c] (‰)	2SD Measured	2SD[d] Reported	n[e]	Fe_{Carb} (wt%)	Fe_{Ox} (wt%)	Fe_{Mag} (wt%)	Fe_{PY} (wt%)	Fe_{HR}[f] (wt%)	Fe_T[g] (wt%)	Fe_{HR}/Fe_T	Fe_{PY}/Fe_{HR}
RC06-FOR01-A	835.84–835.87	5.1	4.8	14	15	2.7	1.15	1.07	0.06	0.15	3	0.1	0.1	0.0	2.7	2.9	2.8	1.00	0.94
RC06-FOR01-B	835.77–835.79	5.6	4.7	14	16	2.5	1.20	1.12	0.10	0.15	3	0.1	0.1	0.0	2.5	2.6	2.6	0.99	0.95
RC06-FOR01-C	835.70–835.72	5.3	5.4	14	14	2.6	1.23	1.15	0.10	0.15	3	0.1	0.1	0.0	3.1	3.3	2.9	1.00	0.96
RC06-FOR01-D	835.65–835.68	5.6	5.1	12	13	2.2	1.18	1.10	0.13	0.15	3	0.1	0.1	0.0	2.6	2.8	2.8	0.98	0.95
RC06-FOR01-E	835.58–835.62	5.3	5.1	12	13	2.3	1.17	1.09	0.06	0.15	3	0.1	0.1	0.0	2.5	2.7	2.6	1.00	0.95
RC06-FOR02-B	828.11–828.15	6.5	7.0	29	22	4.5	0.61	0.53	0.10	0.15	3	0.1	0.1	0.0	3.0	3.3	4.1	0.79	0.93
RC06-FOR02-D	828.23–828.27	6.6	5.7	29	27	4.4	0.63	0.55	0.18	0.18	6	0.1	0.1	0.0	3.0	3.3	4.1	0.80	0.93
RC06-FOR02-G	828.37–828.40	6.5	7.4	33	24	5.1	0.54	0.46	0.21	0.21	6	0.1	0.1	0.0	3.4	3.6	4.5	0.80	0.93
RC06-FOR02-H	828.48–828.50	6.4	5.6	30	29	4.7	0.47	0.39	0.10	0.15	3	0.1	0.1	0.0	3.3	3.6	4.0	0.90	0.93
RC06-FOR02-I	828.55–828.58	6.8	7.3	29	21	4.2	0.62	0.54	0.12	0.15	4	0.1	0.2	0.0	2.9	3.3	4.0	0.81	0.90

[a] TOC = total organic carbon.
[b] Mo isotope data reported relative to RochMo2.
[c] Mo isotope data reported relative to NIST SRM 3134 = 0.25‰.
[d] Uncertainty is the 2SD of replicate measurements or 0.15‰, whichever is greater.
[e] Number of replicate analyses of the same sample solution.
[f] Fe_{HR} = Highly reactive Fe abundance = $Fe_{Carbonate}$ (Fe_{Carb}) + $Fe_{Ferric\text{-}Oxide}$ (Fe_{Ox}) + $Fe_{Magnetite}$ (Fe_{Mag}) + Fe_{Pyrite} (Fe_{PY}).
[g] Fe_T = Total Fe abundance.